NASA TECHNICAL NOTE

NASA TN D-4142

NASA TN D-4142

A WIND-TUNNEL INVESTIGATION OF A 7-FOOT-DIAMETER DUCTED PROPELLER

by Kenneth W. Mort and Berl Gamse

Ames Research Center
Moffett Field, Calif.

NATIONAL AERONAUTICS AND SPACE ADMINISTRATION • WASHINGTON, D. C. • AUGUST 1967

NASA TN D-4142

A WIND-TUNNEL INVESTIGATION OF A 7-FOOT-DIAMETER DUCTED PROPELLER

By Kenneth W. Mort and Berl Gamse

Ames Research Center
Moffett Field, Calif.

NATIONAL AERONAUTICS AND SPACE ADMINISTRATION

For sale by the Clearinghouse for Federal Scientific and Technical Information
Springfield, Virginia 22151 – CFSTI price $3.00

A WIND-TUNNEL INVESTIGATION OF A 7-FOOT-DIAMETER DUCTED PROPELLER

By Kenneth W. Mort and Berl Gamse

Ames Research Center

SUMMARY

Power, free-stream velocity, blade angle, and duct angle of attack were varied to define the aerodynamic characteristics of a full-scale ducted propeller. Dynamic pressure ranged from 0 to 106 psf, rotational velocity from 1200 to 2590 rpm, blade angle from 14° to 49°, and power from 0 to 1250 hp.

The results indicate that the ducted propeller achieved a maximum figure of merit of 81 percent and a maximum propulsive efficiency of 74 percent.

Stall boundaries for both the upstream and downstream duct lips were based on pressure distributions. It was found that for a representative V/STOL configuration employing this ducted fan the upstream lip could stall at low power and at high duct angles; however, stall of the downstream lip did not appear to be likely.

INTRODUCTION

Experimental information concerning the performance of large-scale ducted propellers suitable for lifting and propelling VTOL aircraft has been very meager. Therefore, an investigation of a 7-foot-diameter ducted propeller was made in the Ames 40- by 80-Foot Wind Tunnel.

The test objectives were (1) to define the aerodynamic characteristics of the ducted propeller; (2) to evaluate the propulsive performance; (3) to define the onset of upstream (or lower) and downstream (or upper) duct lip stall; and (4) to define the aerodynamic characteristics of the duct exit vane.

NOTATION

A_e	net exit area, (shroud exit area) minus (exit vane blockage area), ft^2
b	fan blade chord, in.
c	shroud chord, ft

c_{l_i} blade-section design lift coefficients, $\frac{\text{section design lift}}{qb}$

C_D drag coefficients, $\frac{\text{drag}}{qS}$

C_{D_o} drag coefficient at zero lift coefficient

C_f flat-plate skin-friction drag coefficient, $\frac{\text{friction drag}}{(\text{wetted area})q}$

C_L lift coefficient, $\frac{\text{lift}}{qS}$

C_m pitching-moment coefficient, $\frac{m}{qSc}$

C_p power coefficient, $\frac{P}{\rho n^3 d^5}$

C_T thrust coefficient, $\frac{T}{\rho n^2 d^4}$

d propeller diameter, ft

d_e duct exit diameter, ft

FM figure of merit, $50 \frac{d}{\sqrt{A_e}} \frac{C_T^{3/2}}{C_p}$, percent

h fan-blade thickness, in.

J advance ratio, $\frac{V}{nd}$

m pitching moment about duct rotation axis, ft-lb

n propeller rotational speed, rps

N propeller rotational speed, rpm

P power, (ft-lb)/sec

P_c power coefficient, $\frac{P}{qVS}$

P_o power at $\alpha = \delta_v = 0^o$, (ft-lb)/sec

q free-stream dynamic pressure, psf

r radial distance from duct center line, in.

R propeller radius, in.

S reference area, cd_e, ft^2

SHP	input power, hp
T	thrust, lb
T_c	thrust coefficient, $\frac{T_o}{qS}$
T_o	thrust at $\alpha = \delta_v = 0^o$, lb
V	free-stream velocity, fps
V_e	computed velocity at duct exit, fps
V_∞	free-stream velocity, knots
x	chordwise distance from duct leading edge, in.
α	angle of attack, deg
β	propeller blade angle at 3/4 radius station, deg
δ_v	exit vane deflection (see fig. 2(a)), deg
η	propulsive efficiency, $\frac{C_T}{C_p} J \times 100$, percent
ρ	air density, slugs/ft^3

MODEL AND APPARATUS

General Model Description

The ducted propeller model was essentially a full-scale duplicate of those used on the Bell Aerosystems Co. X-22A airplane. The general arrangement of the model in the wind tunnel is shown in figure 1. Model dimensions are given in figure 2 and in table I, and propeller blade characteristics in figure 3.

Propeller Drive System

The propeller was driven by a 1500-hp electric motor through a right-angle gear box. The motor speed could be varied continuously from 0 to 3000 revolutions per minute.

Instrumentation

Forces and moments on the ducted propeller were measured by the wind-tunnel six-component balance. The forces and moments on the wing

fairing and support structure were not transmitted to the balance and hence were not measured. Pressure orifices were located on the shroud in the positions shown in figure 2(b).

The power input to the ducted propeller was determined from the motor output torque and rotational speed. The torque was measured by a strain-gage balance.

TESTS

The propeller blade angle, rotational velocity, and free-stream dynamic pressure were set and the duct angle of attack was varied during the tests. The blade angles ranged from 14° to 49°, the dynamic pressures ranged from 0 to 106 psf, and the rotational velocities ranged from 1200 to 2590 rpm.

During most of the tests the exit vane was in place, but a few tests were made with the vane off. Exit vane deflections from -17° to $+20^\circ$ were examined.

REDUCTION OF DATA

Corrections

No corrections for wind-tunnel wall effects were applied to the data because they were not significant. No corrections were made for gear box losses because they were estimated to be on the order of 1/2 percent of the input power.

Accuracy of Measuring Devices

The various measuring devices used were accurate within the following limits which include errors in reading and reducing the data as well as the errors of the device itself.

Lift	±3 lb
Drag	±3 lb
Pitching moment	±100 ft-lb
Motor input torque	±15 ft-lb
Rotational speed	±0.5 rps
Free-stream dynamic pressure	±0.1 psf for values $\leq$ 20 psf ±1/2 percent for values $\geq$ 20 psf
Angle of attack	$\pm 0.5^\circ$
Propeller blade angle	$\pm 0.5^\circ$
Exit vane deflection	$\pm 2^\circ$

RESULTS AND DISCUSSION

Basic Aerodynamic Characteristics

Thrust and power coefficient results at $\alpha = 0^\circ$.- The ducted fan thrust and power coefficients (C_T and C_p) in figure 4 are for the exit vane installed at zero deflection ($\delta_v = 0^\circ$). The results in figure 5 were obtained with and without the exit vane at $\delta_v = 0^\circ$. The configuration with the exit vane is considered the basic configuration because the amount of duct diffusion selected was based on the presence of the vane. The propulsive efficiency and static efficiency were better with the vane. (The static efficiency was better because at $J = 0$, C_p was the same with and without the vane, while C_T was lower without the exit vane.)

From the results of figure 4 the variations in thrust coefficient appear to be regular for blade angles from 14° to about 39°, but at 44° the value at zero advance ratio is low and remained low until the advance ratio exceeded about 0.7. This was probably because significant portions of the blades were stalled. At 49° the blades appeared to remain stalled until the advance ratio exceeded about 1.

The coefficients in figures 4 and 5 are referenced to rotational velocity. Thrust coefficient referenced to free-stream velocity was determined from the results of figure 4, and is shown in figure 6. This thrust coefficient, T_c, which was obtained at zero angle of attack and zero exit vane deflection, is used in subsequent figures as a correlation parameter instead of advance ratio and blade angle.

Basic aerodynamic characteristics at $\alpha \geq 0^\circ$.- The basic aerodynamic characteristics are presented in figure 7 for several values of T_c.[1] Lift coefficient is plotted as a function of duct angle of attack, drag coefficient, and pitching moment, and power coefficient P_c is plotted as a function of α. The results in figure 7 are for several exit vane deflections and in figure 8 for the exit vane out.

Figure 9 shows the aerodynamic characteristics with the propeller removed and with the exit vane at $\delta_v = 0^\circ$. As shown, the variation of C_D with C_L is consistent with the expression $C_D = C_{D_0} + \frac{C_L^2}{2\pi(d_e/c)}$ to maximum C_L as was found for the small-scale ring wings of reference 1. This suggests that the presence of the exit vane did not affect the induced drag.

[1]The rotational velocity and blade angle at which the test was conducted are also included to allow determination of the actual test conditions if desired.

Evaluation of the Static and Propulsive Efficiency

Efficiency.- The static efficiency and propulsive efficiency computed from the faired curves of figure 4 are presented in figure 10. The static efficiency is shown in figure 10(a) as the figure of merit (based on net exit area) plotted against blade angle. The maximum figure of merit achieved was about 81 percent. The propulsive efficiency is presented in figure 10(b); the maximum achieved was 74 percent.

These values of efficiency were compared with those achieved by the ducted propellers of references 2 and 3. The ducted propeller of reference 2 and the "static" ducted propeller configuration of reference 3 were designed to produce good static efficiency. (The "static" configuration of ref. 3 had a large bellmouth inlet.) The "cruise" ducted fan configuration of reference 3 was designed to produce good high-speed efficiency. Comparison with these models indicated that the 7-foot model achieved very good static efficiency (the model of ref. 2 achieved a figure of merit of 78 percent and the "static" model of ref. 3, 80 percent) and fair propulsive efficiency (the propulsive efficiency of the "cruise" configuration of ref. 3 was 80 percent).

These results suggest that the design of the 7-foot model was a good compromise in satisfying both the low-speed and high-speed design requirements. However, it appears that some improvement in propulsive efficiency should be possible. In the next section the experimental results will be compared with theoretical considerations, and it will be shown that improvements in the propulsive efficiency would necessitate a reduction in the drag of the duct, centerbody, struts, etc.

Comparison with theory.- From the results of figure 4, the maximum thrust which could be achieved was determined as a function of free-stream velocity for a constant input power equal to the design value of 1250 hp. The results are presented in figure 11 with the theoretical thrust for comparison. This theoretical thrust was computed according to "ideal momentum ducted fan theory" using zero duct drag and a propeller efficiency of 90 percent based on the air velocity at the propeller. (This efficiency is an average, over the velocity range shown, of the values estimated using ref. 4. The estimated variation over the velocity range was about ±3 percent.) For free-stream velocities up to about 100 knots the thrust obtained experimentally follows the ideal curve reasonably well. However, as velocity is increased further the difference between the experimental curve and ideal curve increases because of the drag of the duct, centerbody, strut, etc. This is shown in figure 11 by a curve which was obtained by subtracting the propeller-out drag data of figure 9 from the ideal curve.[2] The resulting curve compares rather well with the experimental thrust curve. Hence, it may be concluded that the drag of the duct, centerbody, struts, etc., causes the reduction in thrust shown at high forward speeds. It may also be concluded that the propeller

[2]The increase in drag due to the higher internal velocity when the propeller is present is negligible compared to the total duct drag. Hence, the propeller-out drag is representative of the total duct drag with the propeller present.

efficiency is approximately 90 percent as was assumed since the measured thrust agrees well with that predicted using a propeller efficiency of 90 percent and propeller-out duct drag.

To estimate how much of the drag in figure 11 was due to shroud friction, the friction drag of the shroud was estimated and an increment subtracted from the ideal curve. The resulting curve, also shown in figure 11, represents the best possible thrust which could be approached if the ducted propeller were designed exclusively for high speed. Because of the large difference between this curve and the experimental curve, it is evident that the major portion of the experimentally determined drag is not due to shroud friction drag, and suggests the possibility for making large reductions in drag and hence increasing the propulsive efficiency.

Examination of the Exit Vane Performance

The exit vane aerodynamic characteristics at zero free-stream velocity are presented in figure 12 by showing lift, thrust, pitching moment, and power as functions of δ_v. The exit vane performance for free-stream velocities greater than zero was determined from the results of figure 7 and is presented in figure 13 for four values of T_c. Here ΔC_L, ΔC_D, ΔC_m, and ΔP_c are shown as functions of δ_v. These results may be analyzed assuming the vane causes a linear variation in the force normal to the duct axis. This force can then be resolved in the lift and drag directions. If this is done it is found that at negative values of δ_v the ΔC_L and ΔC_D variations with δ_v are greater than would be expected. However, at positive values of δ_v the ΔC_L and ΔC_D variations with δ_v are less than would be expected as α is increased. For example, at $T_c = 5$ and $\alpha = 50^\circ$, ΔC_L is essentially zero for positive values of δ_v. The variation in ΔC_m with δ_v in the results of figure 13 is small and hence less important than that for ΔC_L and ΔC_D, particularly if the moment reference is very far from the ducted fan as for the four ducted propeller V/STOL configuration of references 5 and 6.

Duct Lip Stall

Stall of both the upstream (or lower) duct lip and downstream (or upper) duct lip was investigated. Stall of the upstream lip is of primary concern because it is more heavily loaded and would result in a larger reduction in lift when stalled. In addition, stall of this lip affects the propeller loading asymmetrically. Stall of this lip will be considered first and in more detail.

Upstream or lower lip stall.- Flow separation was established on the basis of pressure distributions. A sample is shown in figure 14. As can be seen, separation occurred initially on the inside surface very close to the propeller. As angle of attack was increased the separated area increased forward until finally the flow separated over the entire upstream lip. In figure 15(a) the angle of attack at which separation initially occurred and the angle of attack at which the flow separated over the entire upstream lip are shown as functions of the reciprocal of T_c. This correlation was

obtained for blade angles of 19° and 29° and is considered valid for all blade angles between these values. On examination, the data in figure 7 show that no large changes in forces, moments, and power accompanied the onset of local flow separation, but did accompany separation of the entire lip.

The propeller blade stresses were monitored during the investigation of lip stall. With the onset of flow separation there was only a small rise in stress level. As the angle of attack was increased, the stresses increased gradually. With the entire upstream lip stalled the stresses were still well below critical.

The angle of attack at which separation occurred on the entire upstream lip is shown in figure 15(b) for the present tests and for the small-scale results of references 6 and 7. (The 4-foot model of reference 7 was not a scaled model of the 7-foot model, but the contour of this duct is very similar as the drawings show.) The flow over the entire lip of the 7-foot model and the 4-foot model separated at very nearly the same angle of attack, but there is a large difference between the results shown for the large-scale models and those for the 1/5-scale model. The difference indicates a large-scale effect and suggests that there is a critical lip radius above which increases in radius do not delay separation significantly and below which separation will occur at much lower duct angles of attack.

Downstream or upper lip stall.- Occurrence of separation on the downstream duct lip was also determined from pressure distributions. The angle of attack at which separation occurred over the entire downstream lip is shown in figure 16. In addition, the small-scale results of reference 6 are presented. These results also indicate a large-scale effect. (A stall boundary for the downstream lip was not established for the model of ref. 7.) The data in figure 7 indicate that separation on this lip was not accompanied by any detectable changes in forces, moments, and power nor was buffeting evident during these tests. Consequently, separation on the downstream lip was not considered nearly as critical as separation on the upstream duct lip.

Significance of lip stall boundaries.- The significance of the duct lip stall boundaries is examined in figure 17 which presents duct angle of attack as a function of forward velocity for the four ducted propeller V/STOL configuration of references 5 and 6. The duct angle of attack for trimmed conditions was obtained using a lift force of 3750 pounds (one-fourth of the design gross weight of 15,000 lb). The lift and drag of the vehicle exclusive of the ducted propellers were neglected, equal duct angles were assumed, and trim drag was neglected. The effect of these assumptions is small for this vehicle at the low velocities where the lip may stall. In addition to the trim curve, the curves at which lip stall occurs are shown. From these results it can be concluded that upstream duct lip separation may occur on the simulated vehicle in level flight. However, complete separation of this lip will not occur. (Of course, at low power and at high duct angles, as in descending flight, complete separation of the upstream lip may occur.) Downstream lip stall probably would not be encountered by this type of vehicle.

CONCLUDING REMARKS

The ducted propeller had a maximum figure of merit of 81 percent and a maximum propulsive efficiency of about 74 percent. If the shroud, centerbody, struts, etc., had been designed primarily for high forward velocities, this propulsive efficiency could have been significantly higher. This can be concluded from the fact that the drag with the propeller out was significantly higher than the estimated shroud friction drag. (The friction drag of the other components is small compared to that of the shroud.)

Examination of the exit vane aerodynamic characteristics indicated that at positive vane deflections the variations in C_L and C_D with vane deflection were significantly lower than would be expected as the angle of attack was increased.

Stall of both the upstream and downstream duct lips was examined. The significance of the stall was examined for a four ducted propeller V/STOL configuration employing this ducted propeller. It was found that the onset of flow separation on the upstream lip will be encountered; however, complete separation on this lip will be encountered only during conditions of low power and high duct angle of attack corresponding to high rates of descent. Flow separation on the downstream lip would probably not be encountered by this type of vehicle.

Ames Research Center
National Aeronautics and Space Administration
Moffett Field, Calif., 94035, June 6, 1967
721-03-00-05-00-21

REFERENCES

1. Fletcher, Herman S.: Experimental Investigation of Lift, Drag, and Pitching Moment of Five Annular Airfoils. NACA TN 4117, 1957.

2. Mort, Kenneth W.: Performance Characteristics of a 4-Foot-Diameter Ducted Fan at Zero Angle of Attack for Several Fan Blade Angles. NASA TN D-3122, 1965.

3. Grose, Ronald M.: Wind Tunnel Tests of Shrouded Propellers at Mach Numbers From 0 to 0.60. WADC TR 58-604, United Aircraft Corp., 1958.

4. Anon.: Generalized Method of Shrouded Propeller Performance Estimation. Hamilton Standard Division of United Aircraft Corporation. Publication number PDB 6220.

5. Giulianetti, Demo J.; Biggers, James C.; and Maki, Ralph L.: Longitudinal and Lateral-Directional Aerodynamic Characteristics of a Large-Scale, V/STOL Model With Four Tilting Ducted Fans Arranged in a Dual Tandem Configuration. NASA TN D-3490, 1966.

6. Spreemann, Kenneth P.: Wind-Tunnel Investigation of Longitudinal Aerodynamic Characteristics of a Powered Four-Duct-Propeller VTOL Model in Transition. NASA TN D-3192, 1966.

7. Mort, Kenneth W.; and Yaggy, Paul F.: Aerodynamic Characteristics of a 4-Foot-Diameter Ducted Fan Mounted on the Tip of a Semispan Wing. NASA TN D-1301, 1962.

TABLE I.- BASIC DIMENSIONS OF DUCTED PROPELLER

Duct	
Inside diameter at propeller, in.	84.75
Maximum external diameter, in.	101.56
Chord, in.	49
Exit diameter, in.	93.3
Net exit area, sq ft	44.08
Net area at propeller, sq ft	37.84
Duct rotation station, percent of duct chord	64
Propeller station, percent of duct chord	28.6
Propeller	
Diameter, ft	7
Tip clearance, in.	0.4
Number of blades	3
Integrated design lift coefficient	0.43
Total activity factor	504
Exit vane	
Area, sq ft	31.8
Thickness, in.	5.3
Hinge line, percent of duct chord	85.2

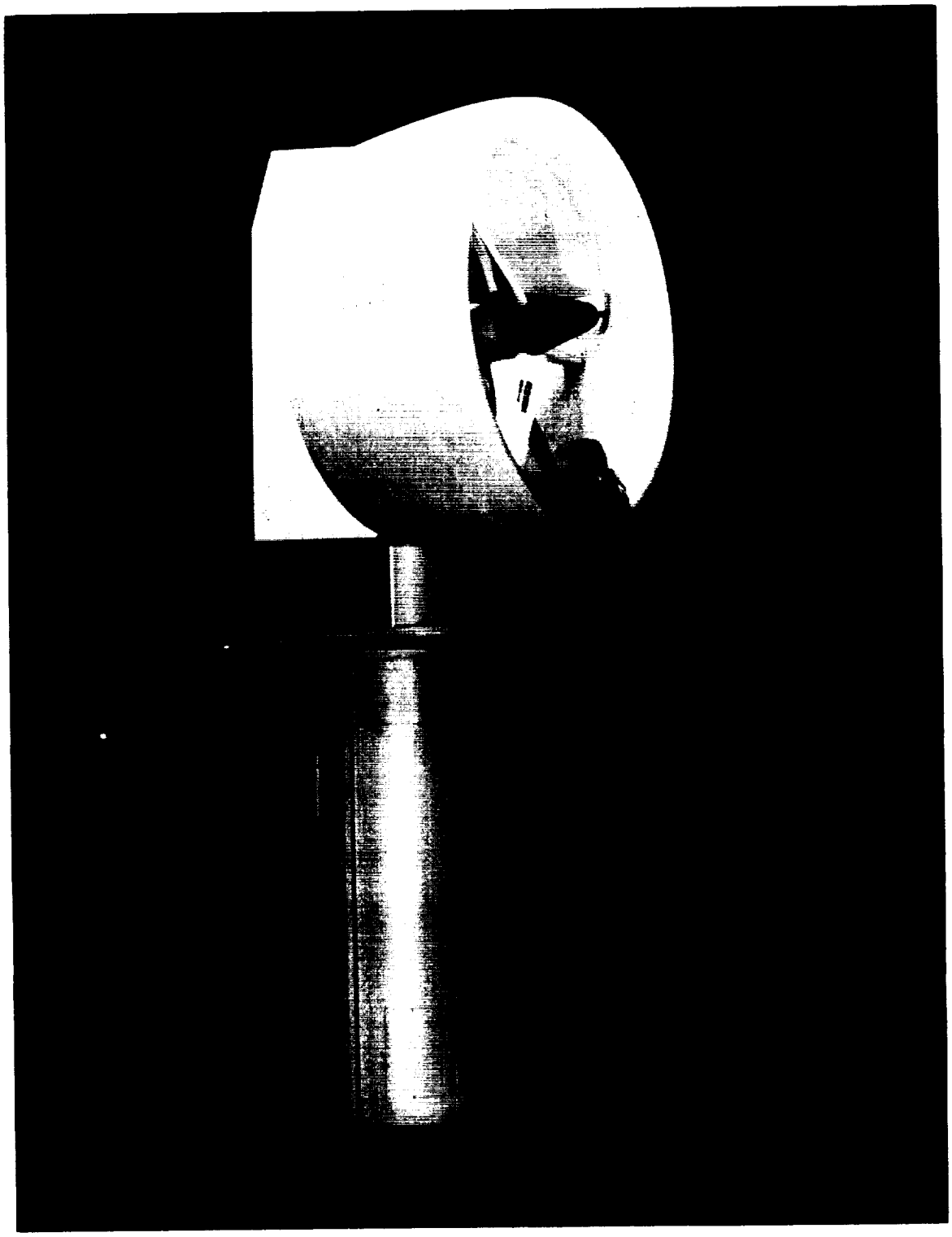

A-32844

(a) 3/4 front view with duct at 90° angle of attack.

Figure 1.- X-22A ducted propeller model mounted in the Ames 40- by 80-Foot Wind Tunnel.

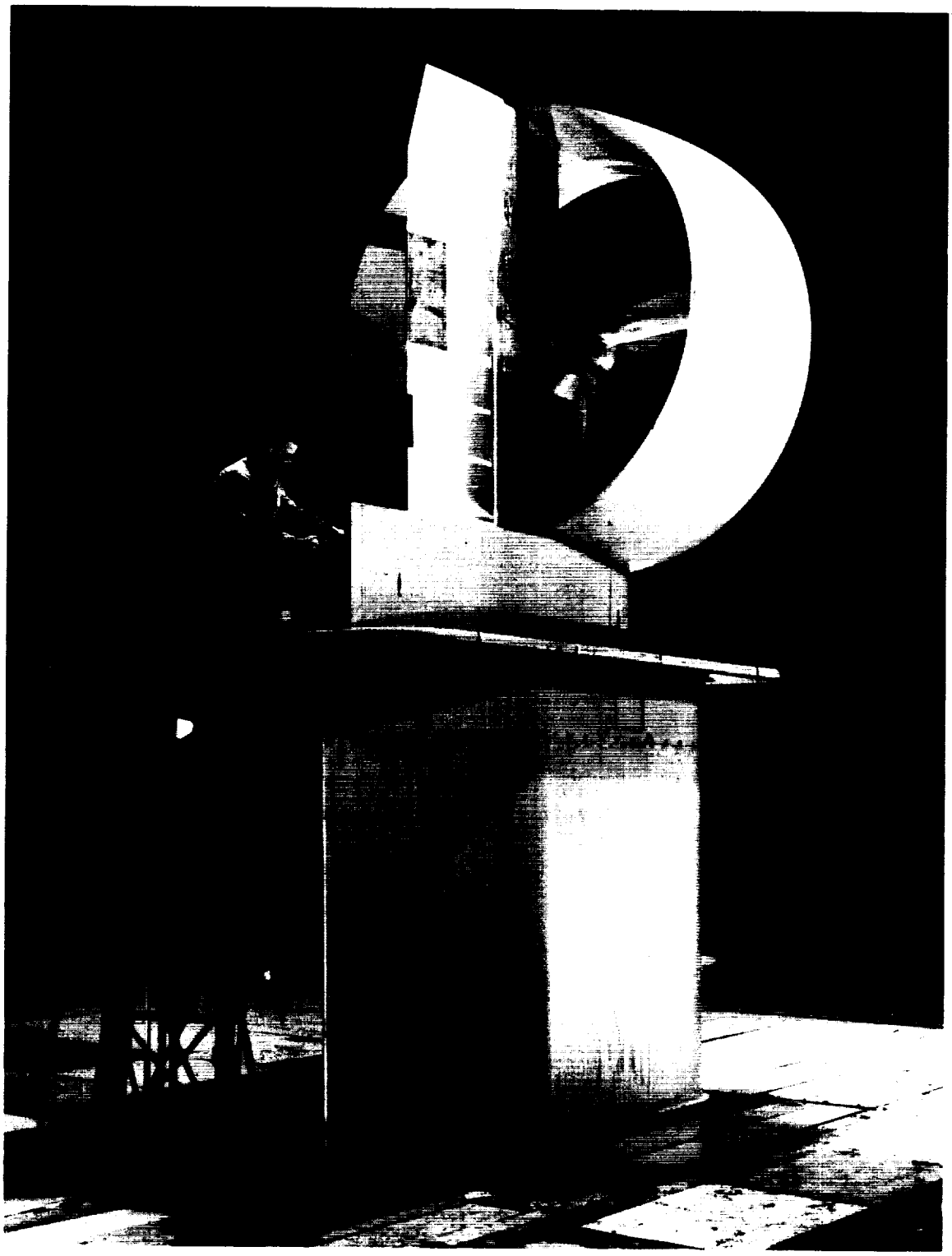

(b) 3/4 rear view with duct at 0° angle of attack. A-33771

Figure 1.- Concluded.

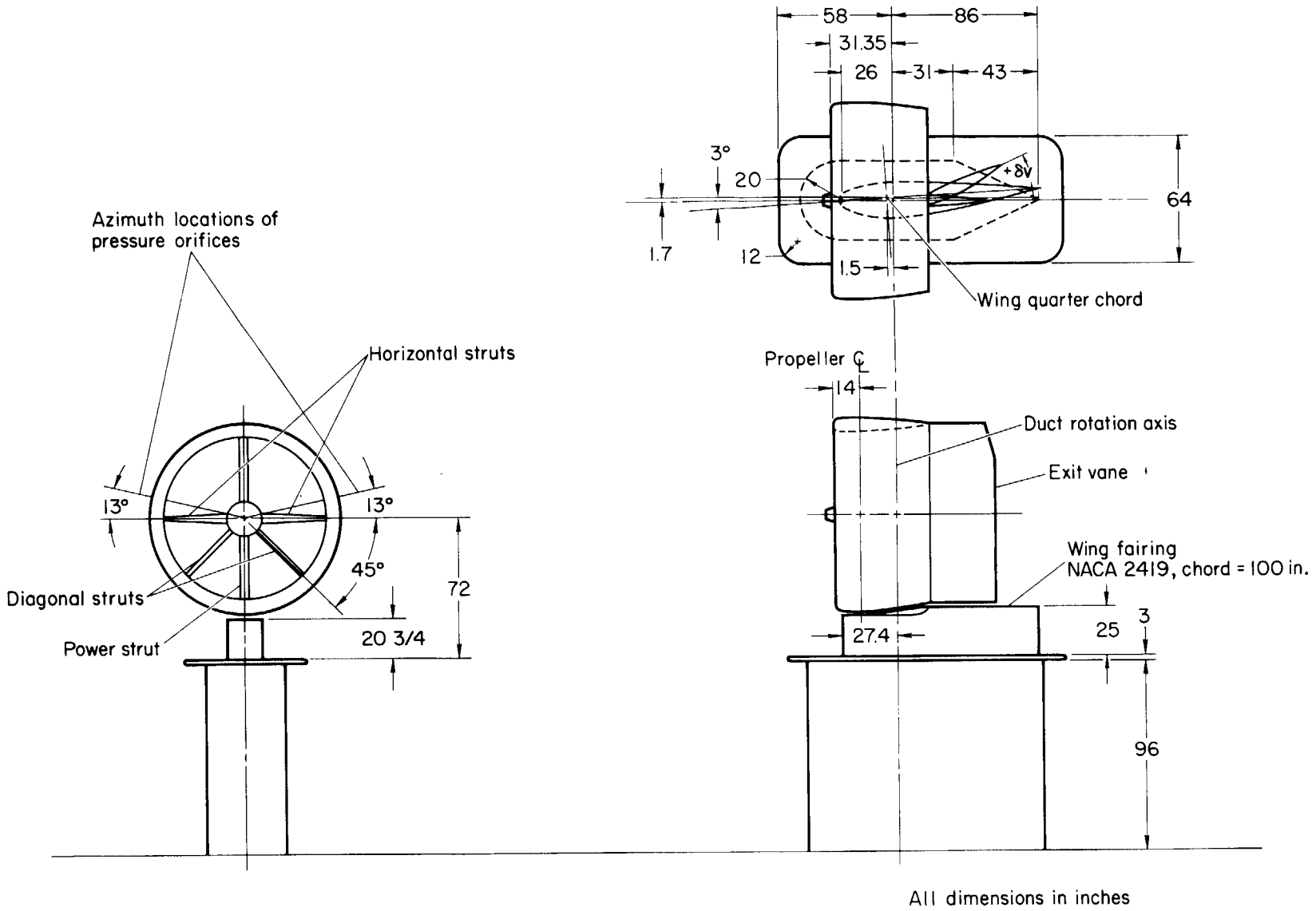

(a) Basic arrangement.

Figure 2.- Model dimensions.

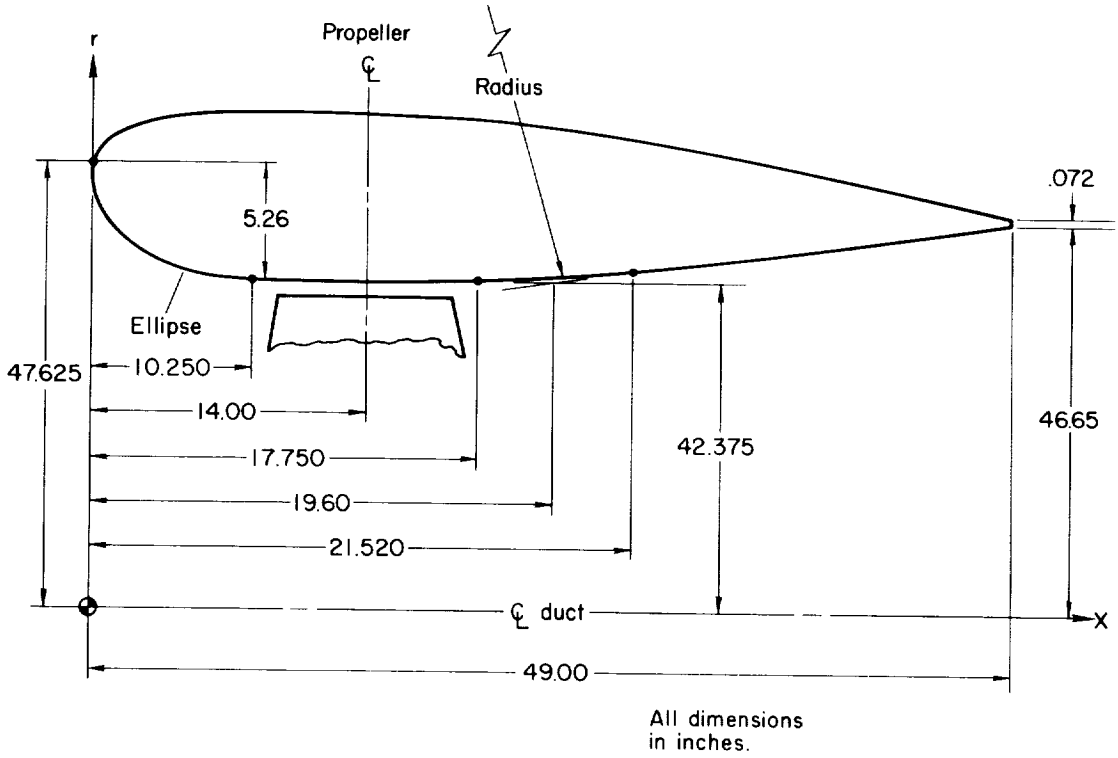

Outside surface ordinates	
X	r
0	47.625
.613	48.695
1.225	49.096
2.450	49.609
3.675	49.953
4.900	50.205
7.350	50.535
9.800	50.710
10.250	—
12.250	50.779
14.700	50.763
17.750	—
19.600	50.552
23.700	—
24.500	50.164
29.400	49.649
34.300	49.038
39.200	49.344
44.100	47.576
46.550	47.160
49.000	46.722

Pressure orifice location		
Number	Location, percent chord	
	Inside	Outside
1	0	
2	1	
3	2.5	
4	5	
5	10	
6	15	
7	25	
8	35	
9	50	
10	70	
11	90	
12		90
13		70
14		50
15		35
16		25
17		15
18		5
19		1.8

(b) Shroud dimensions.

Figure 2.- Continued.

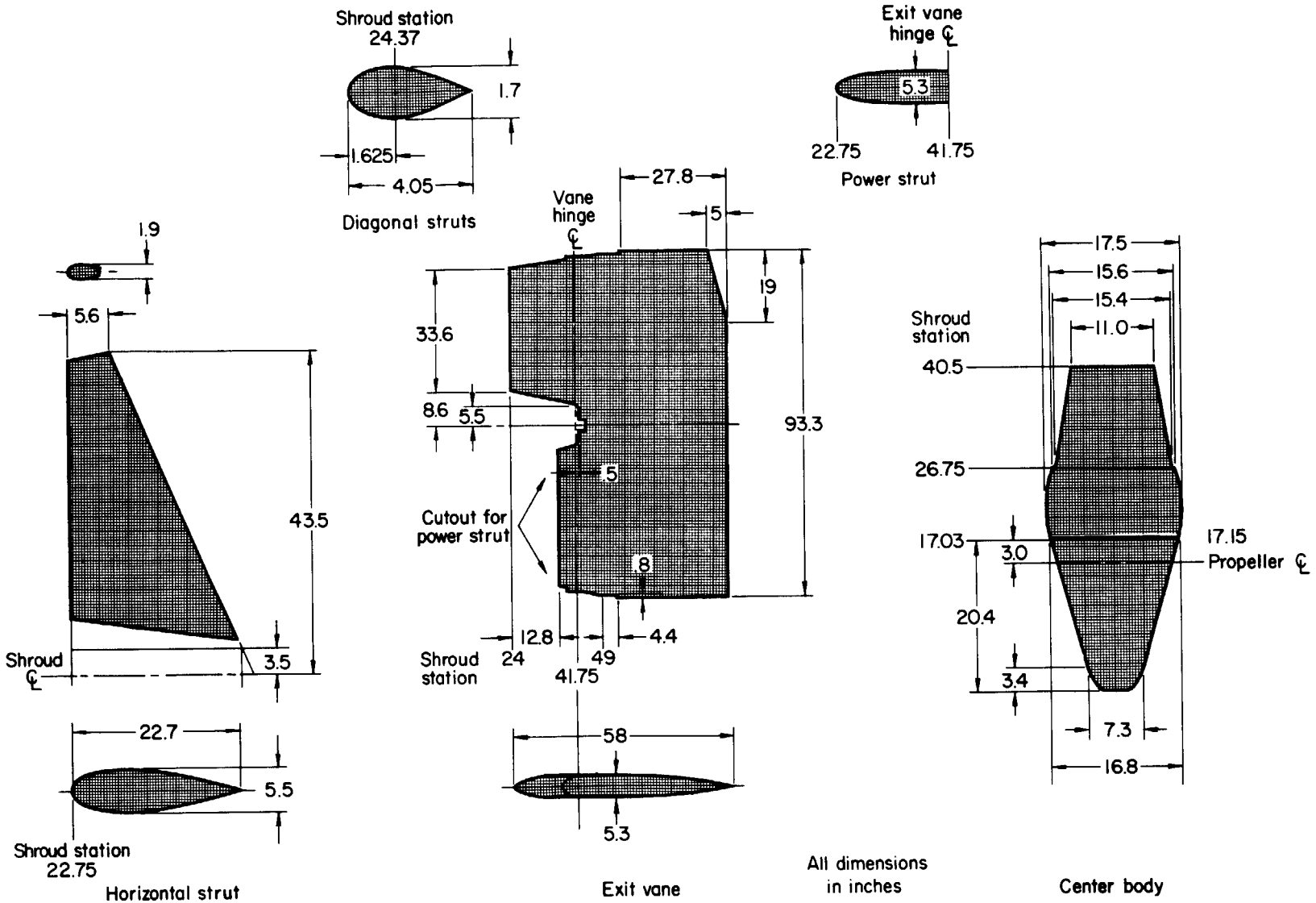

(c) Details of struts, exit vane, and centerbody.

Figure 2.- Concluded.

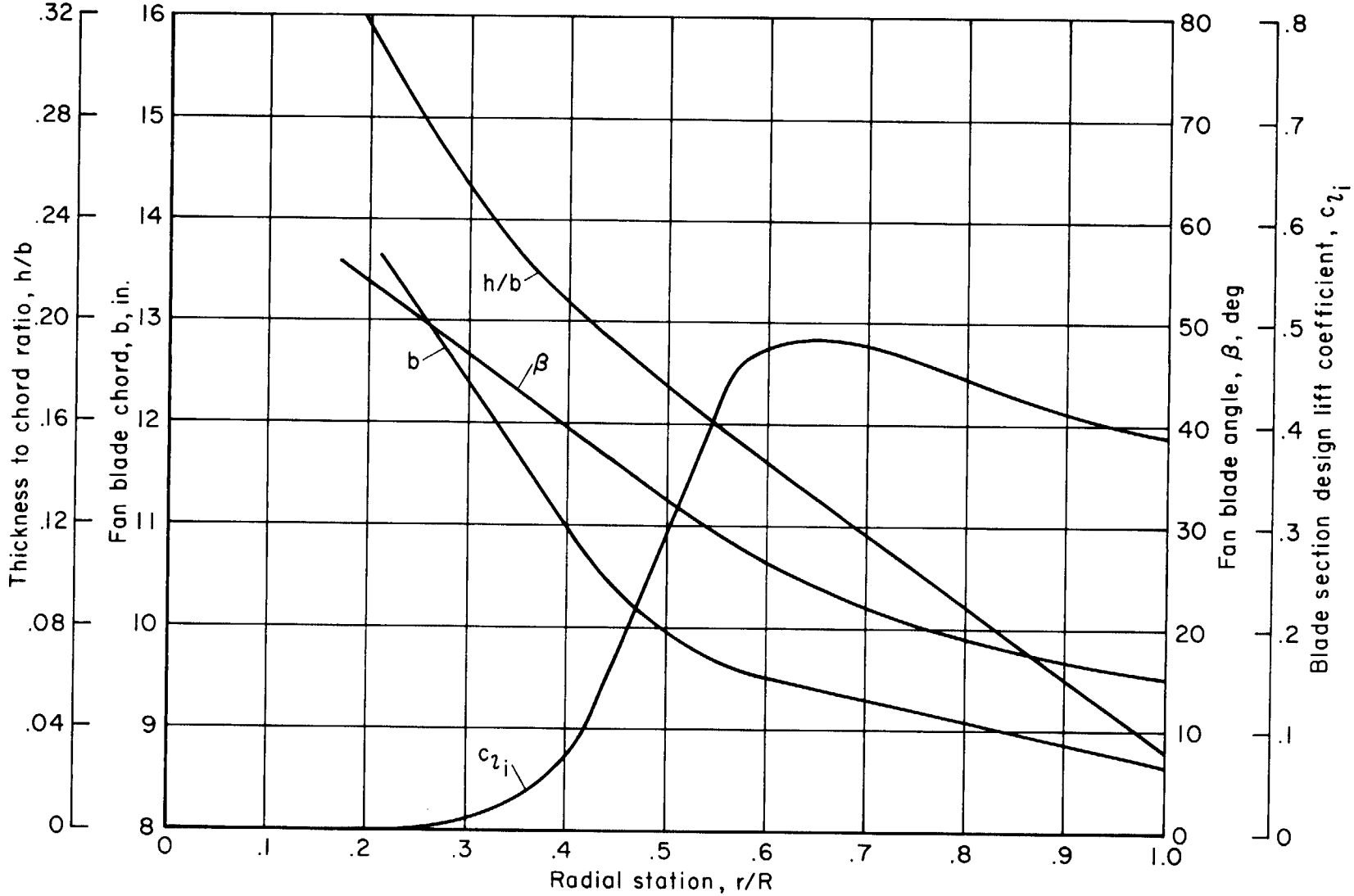

Figure 3.- Propeller blade characteristics with the design lift coefficient, blade chord, blade angle, and blade thickness to chord ratio as functions of the radial distance from the duct center.

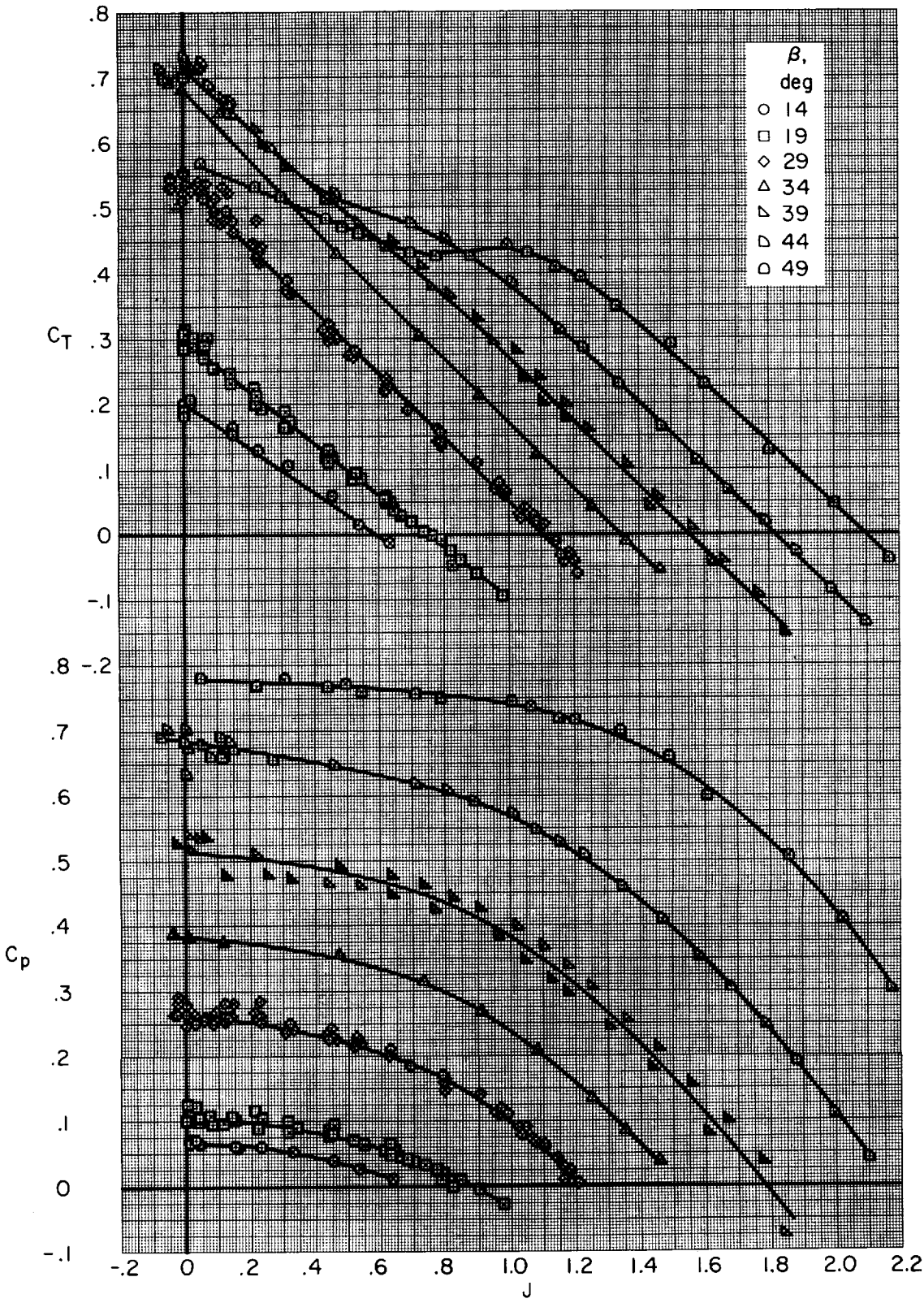

Figure 4.- Ducted propeller thrust and power coefficient referenced to rotational velocity with the exit vane; $\delta_v = \alpha = 0^o$.

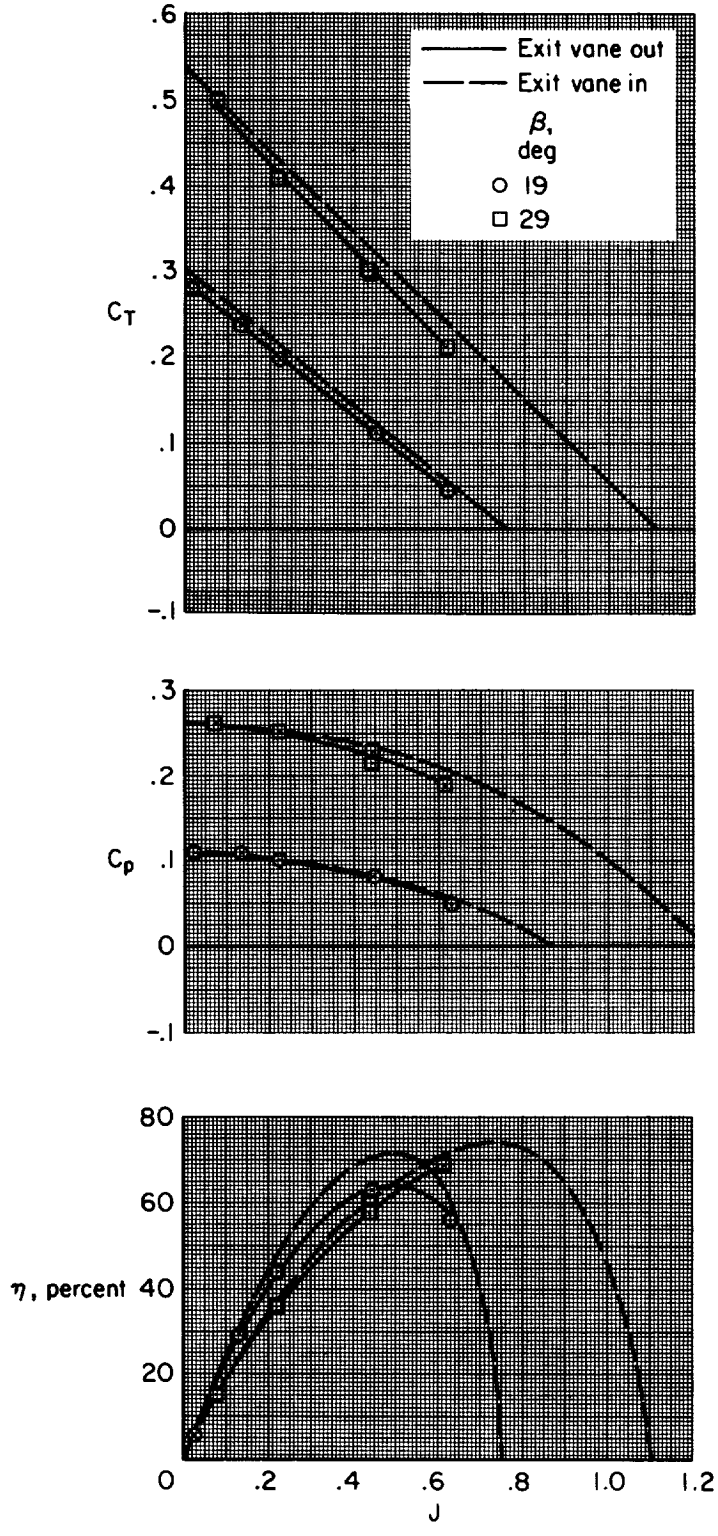

Figure 5.- Ducted propeller thrust and power coefficient and propulsive efficiency with and without the exit vane at $\delta_v = \alpha = 0^\circ$.

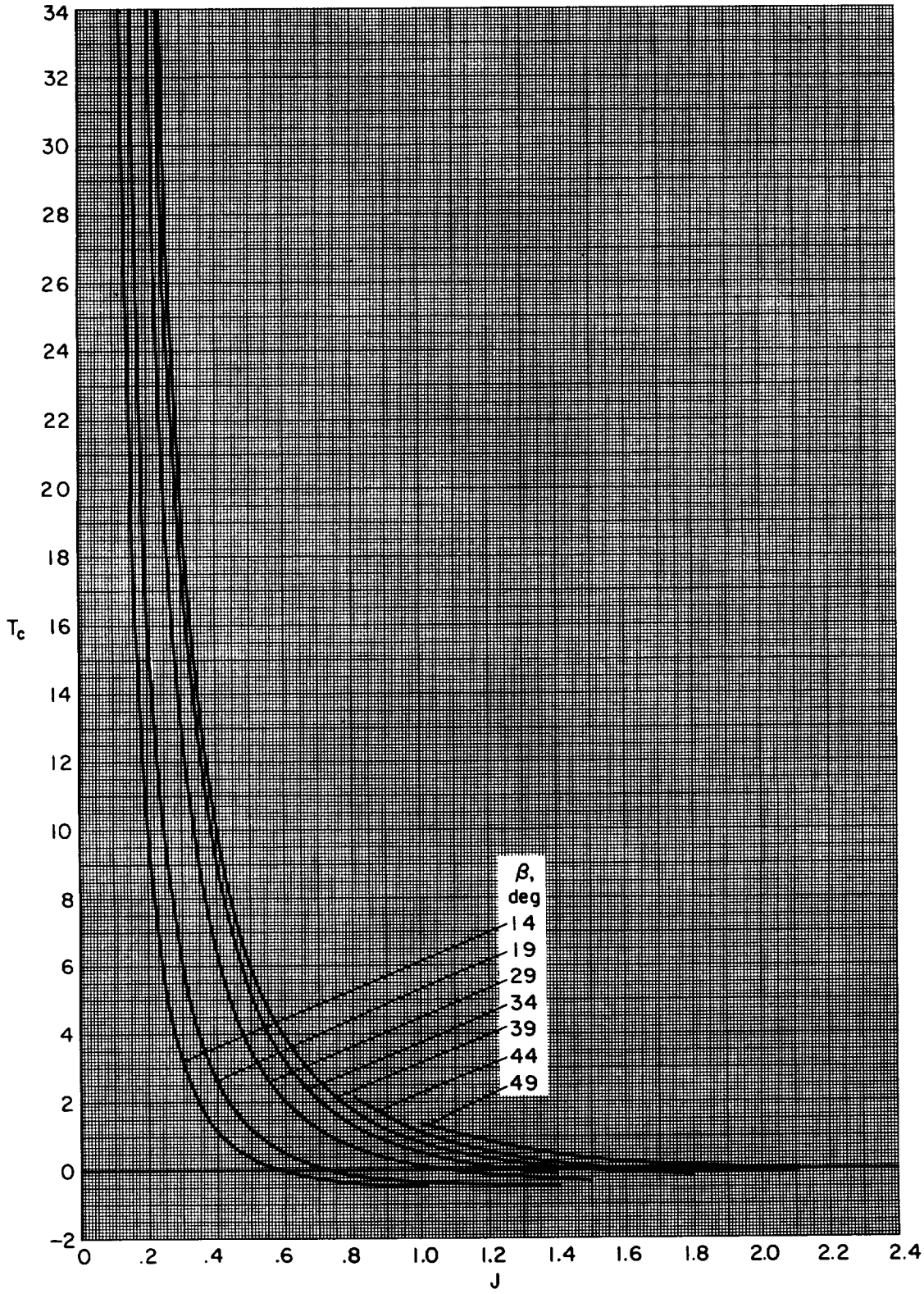

Figure 6.- Thrust coefficient referenced to free-stream velocity; $\delta_v = \alpha = 0^o$.

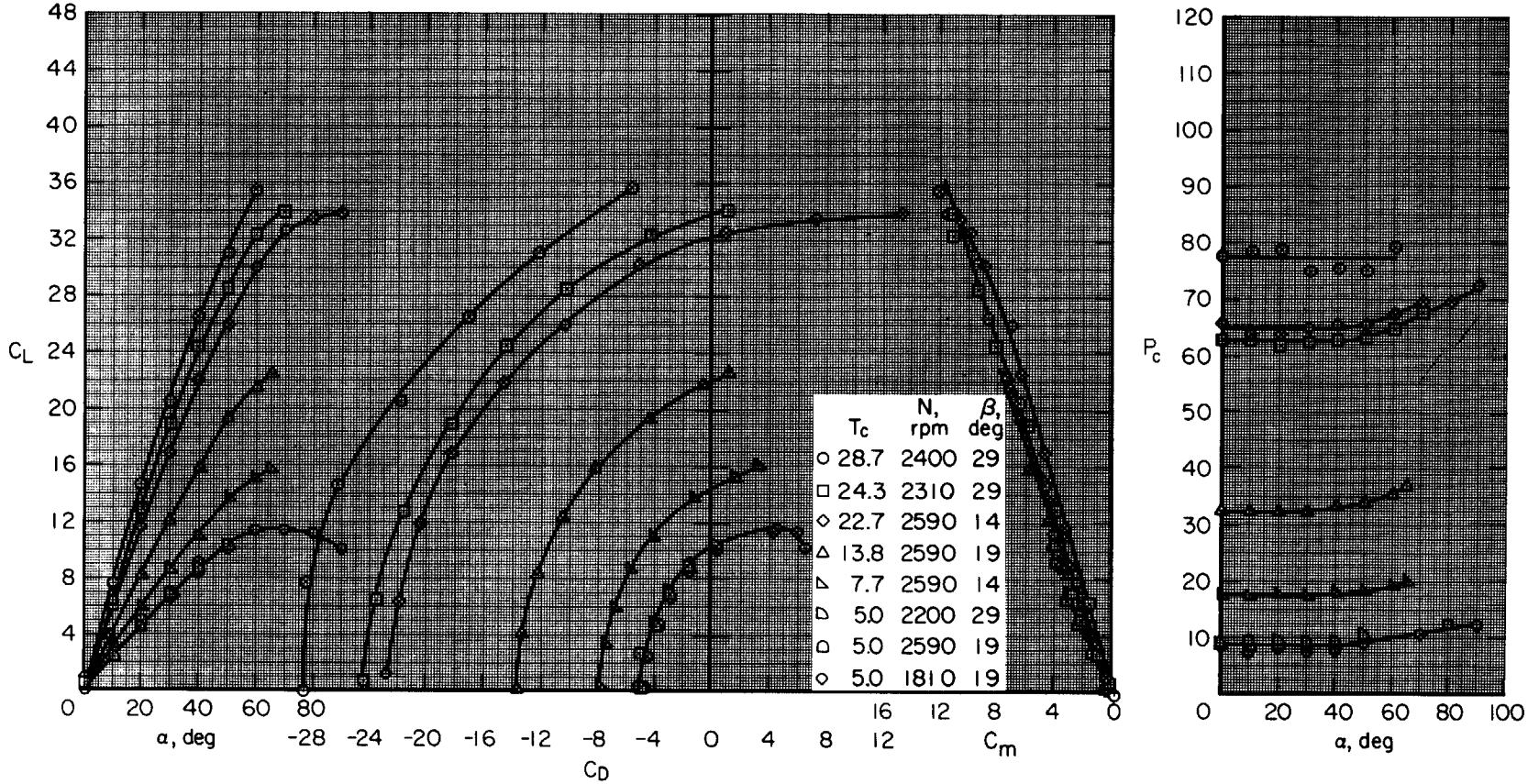

(a) $\delta_v = 0^o$

Figure 7.- Aerodynamic characteristics for several exit vane settings.

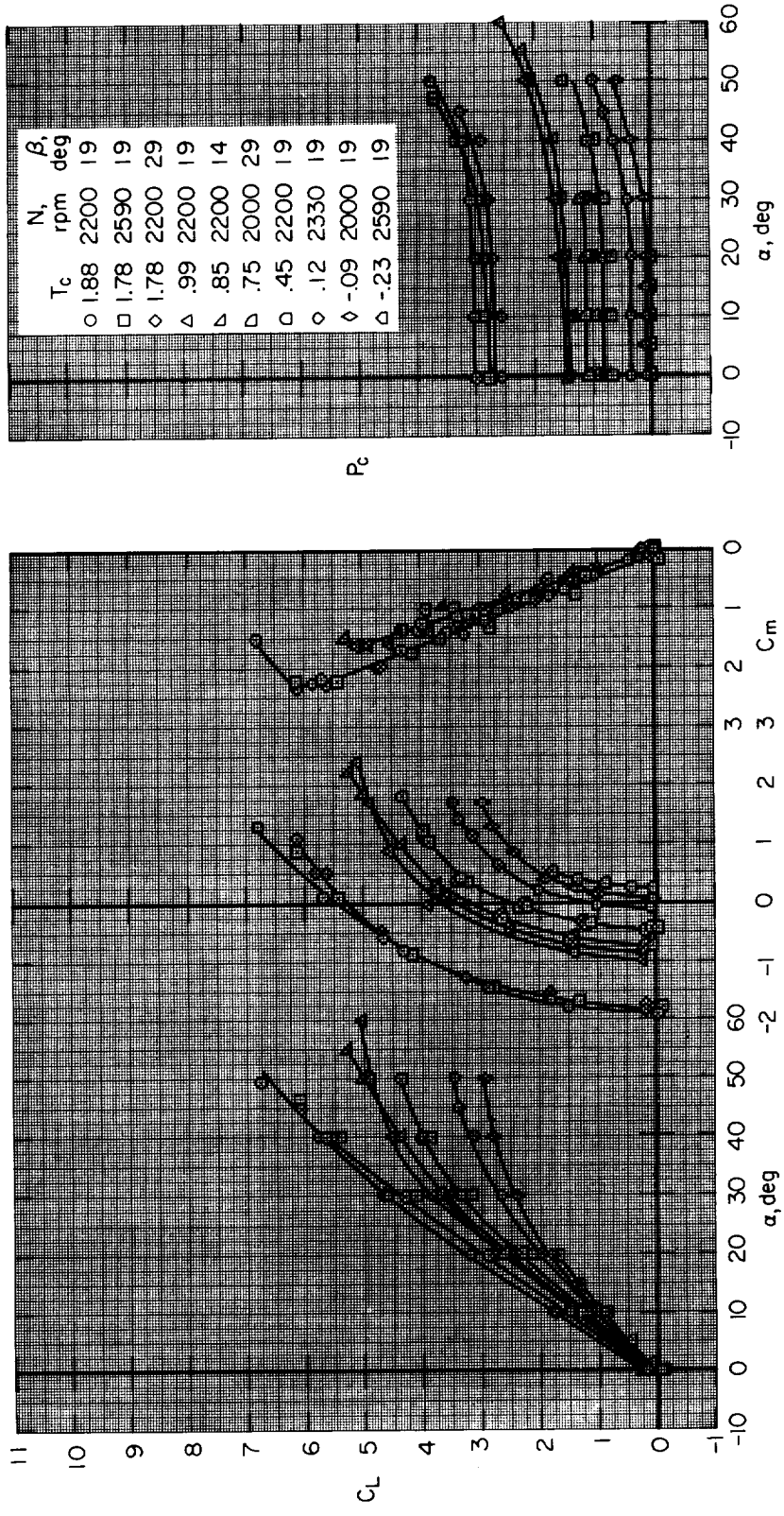

(a) $\delta_V = 0^o$ - Concluded.

Figure 7.- Continued.

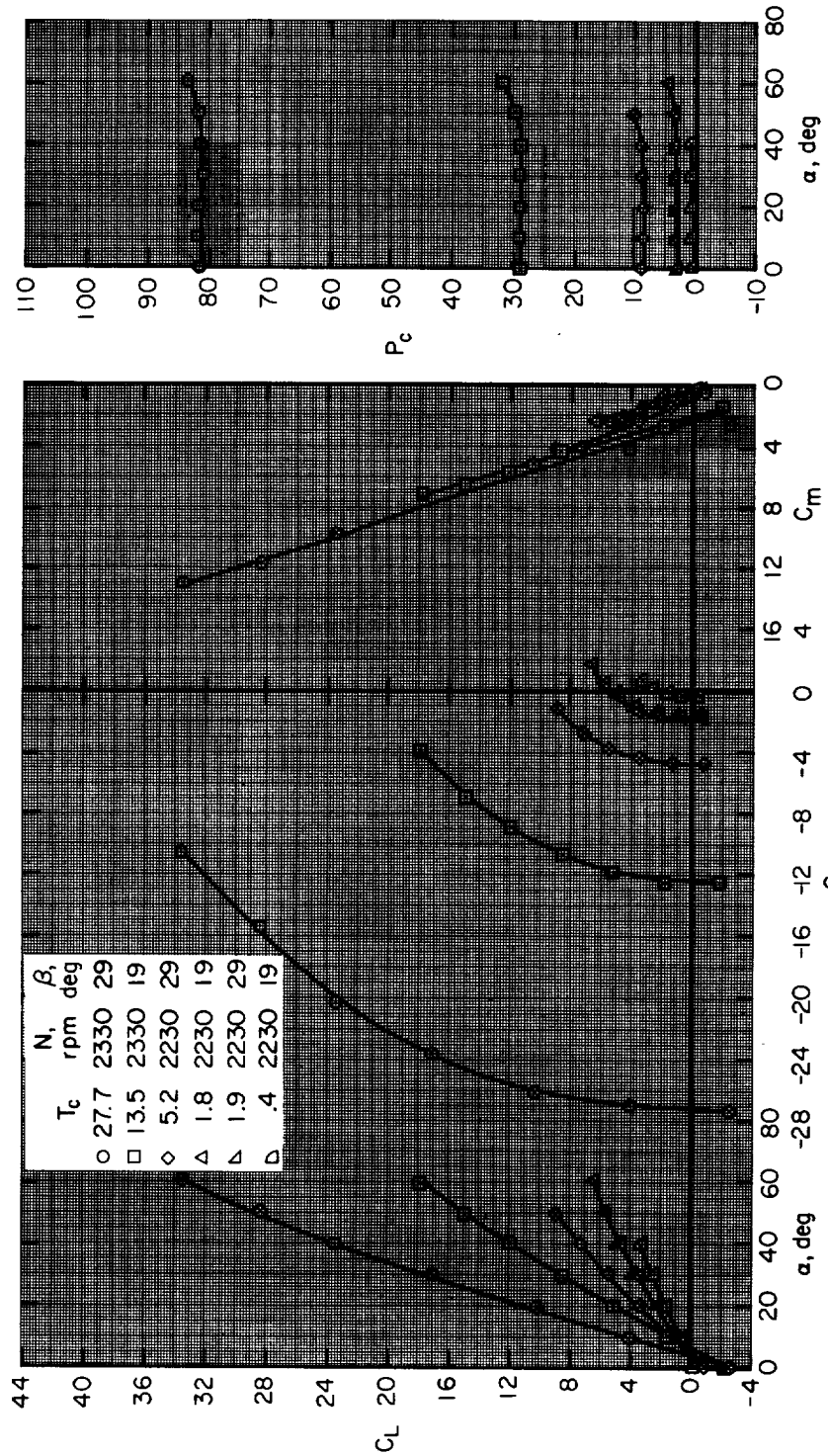

(b) $\delta_V = -17^\circ$

Figure 7.- Continued.

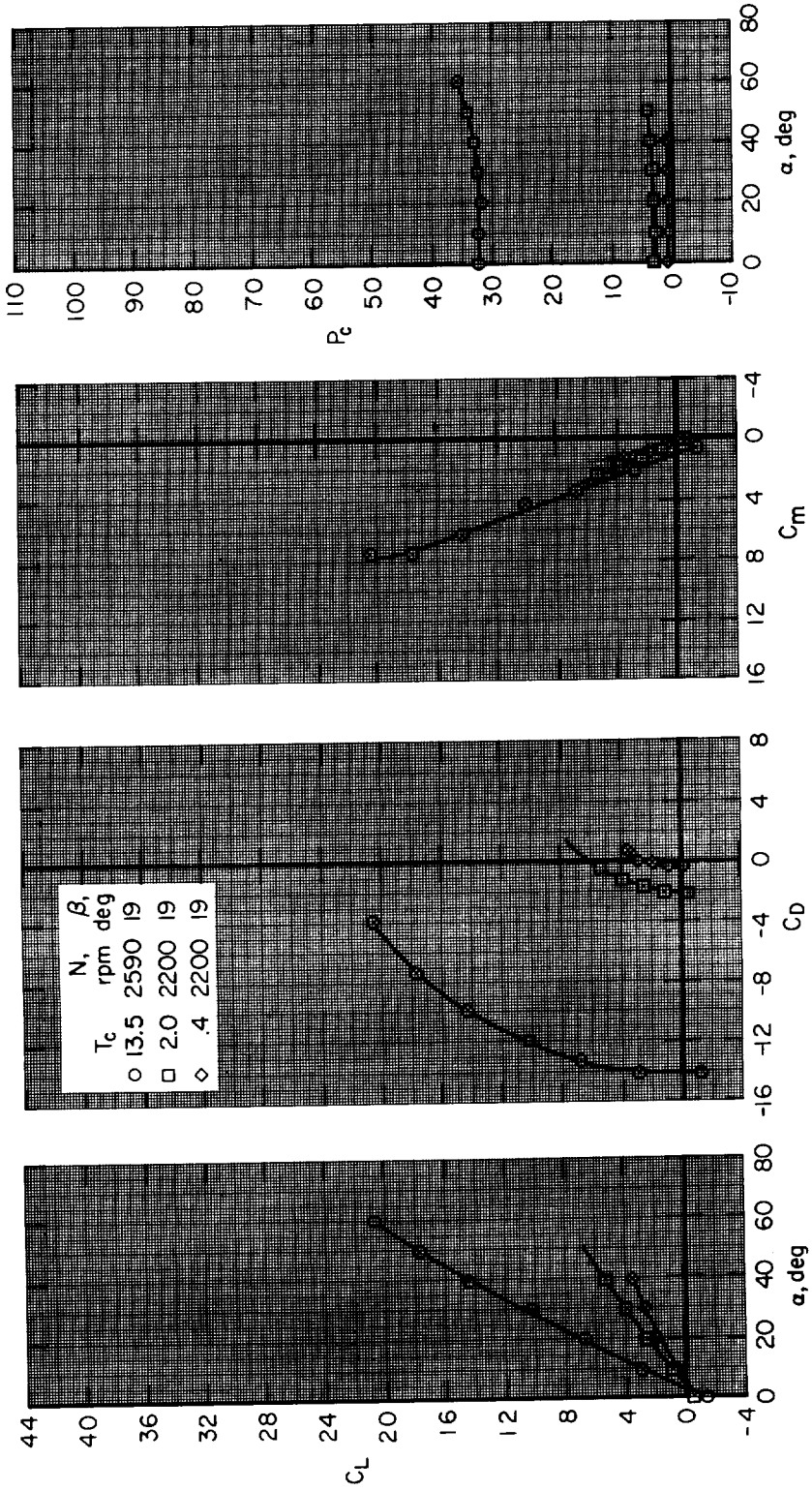

(c) $\delta_V = -10^\circ$

Figure 7.- Continued.

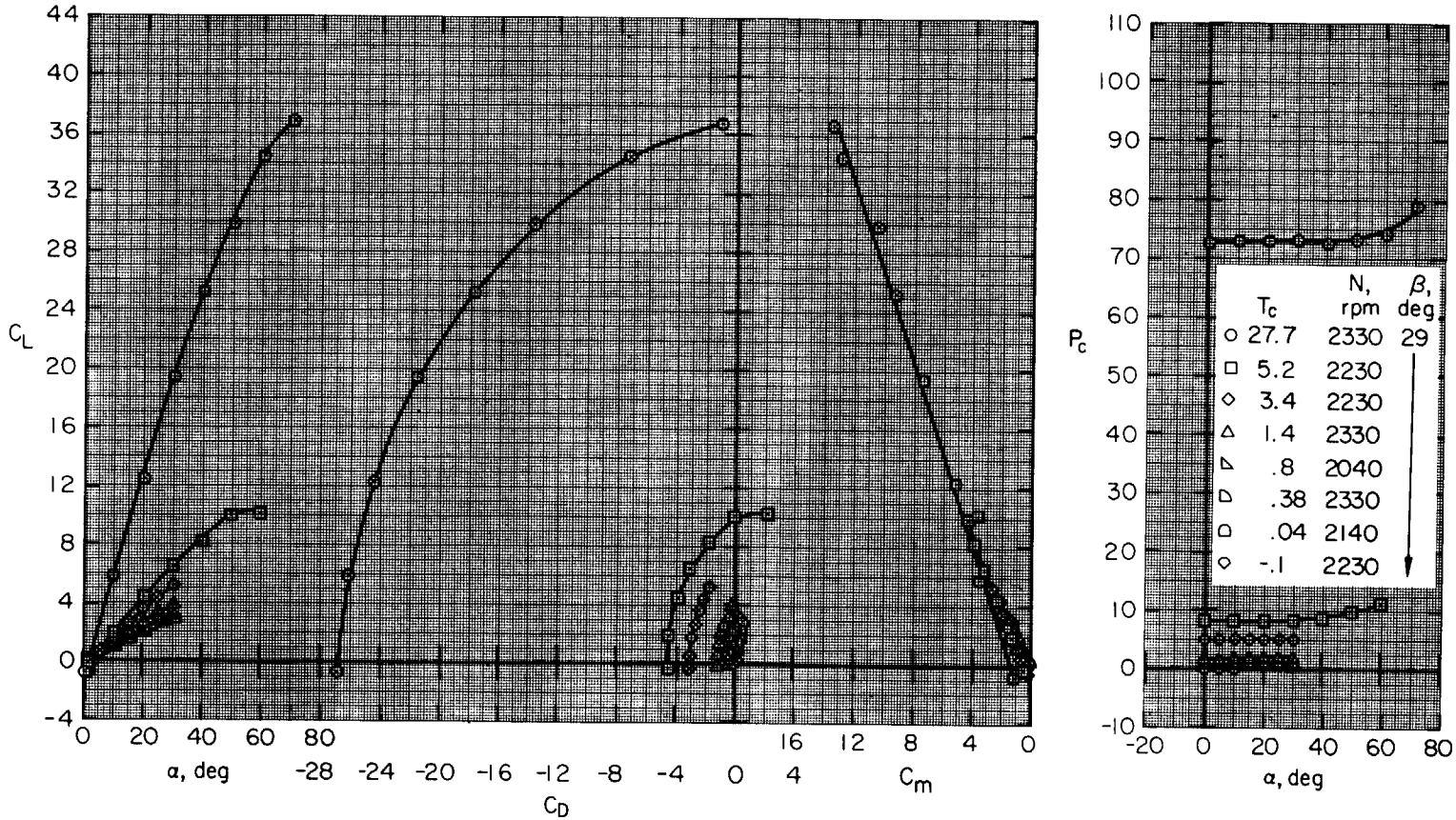

(d) $\delta_v = -7^o$

Figure 7.- Continued.

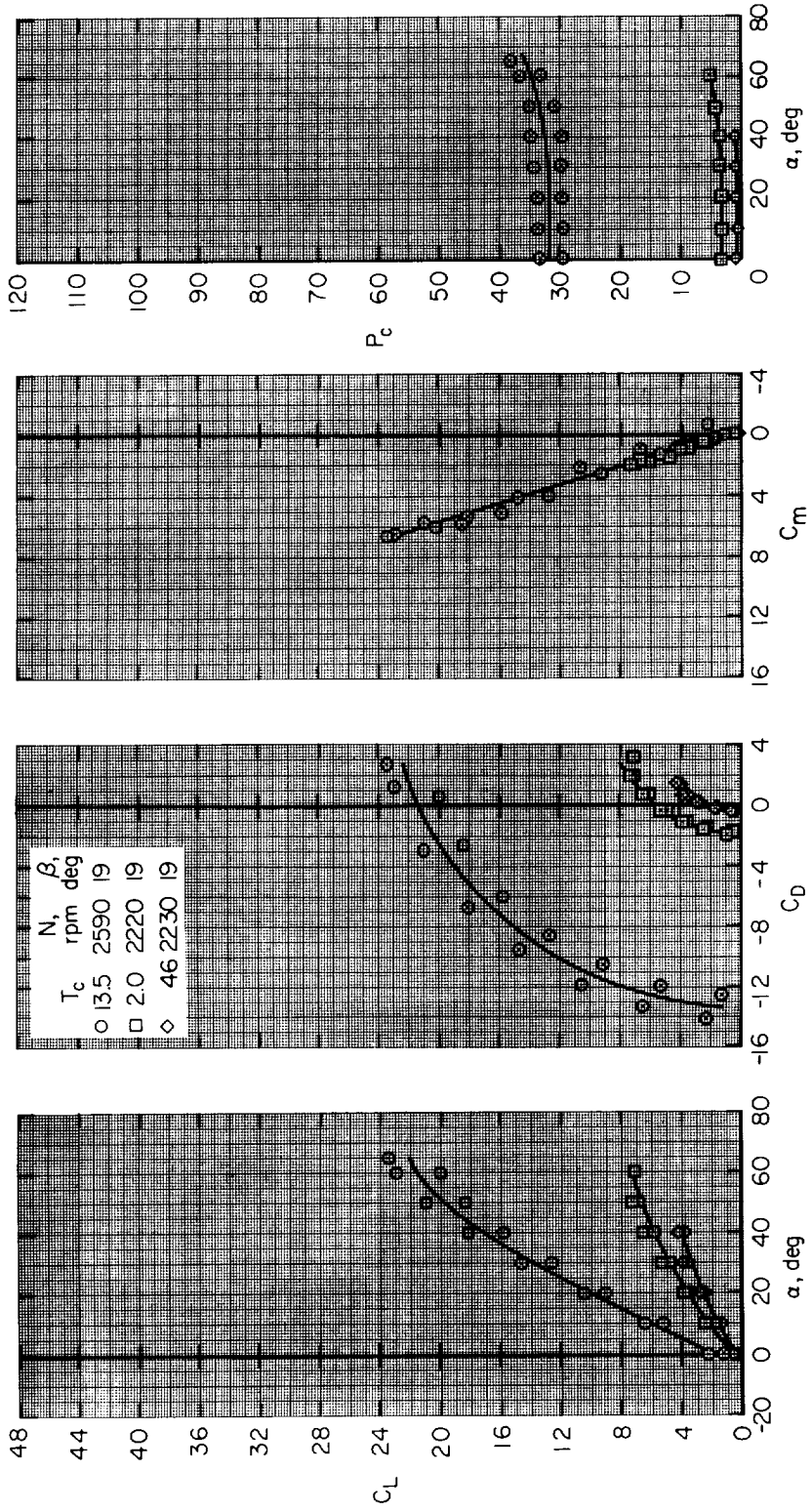

(e) $\delta_r = 10^\circ$

Figure 7.- Continued.

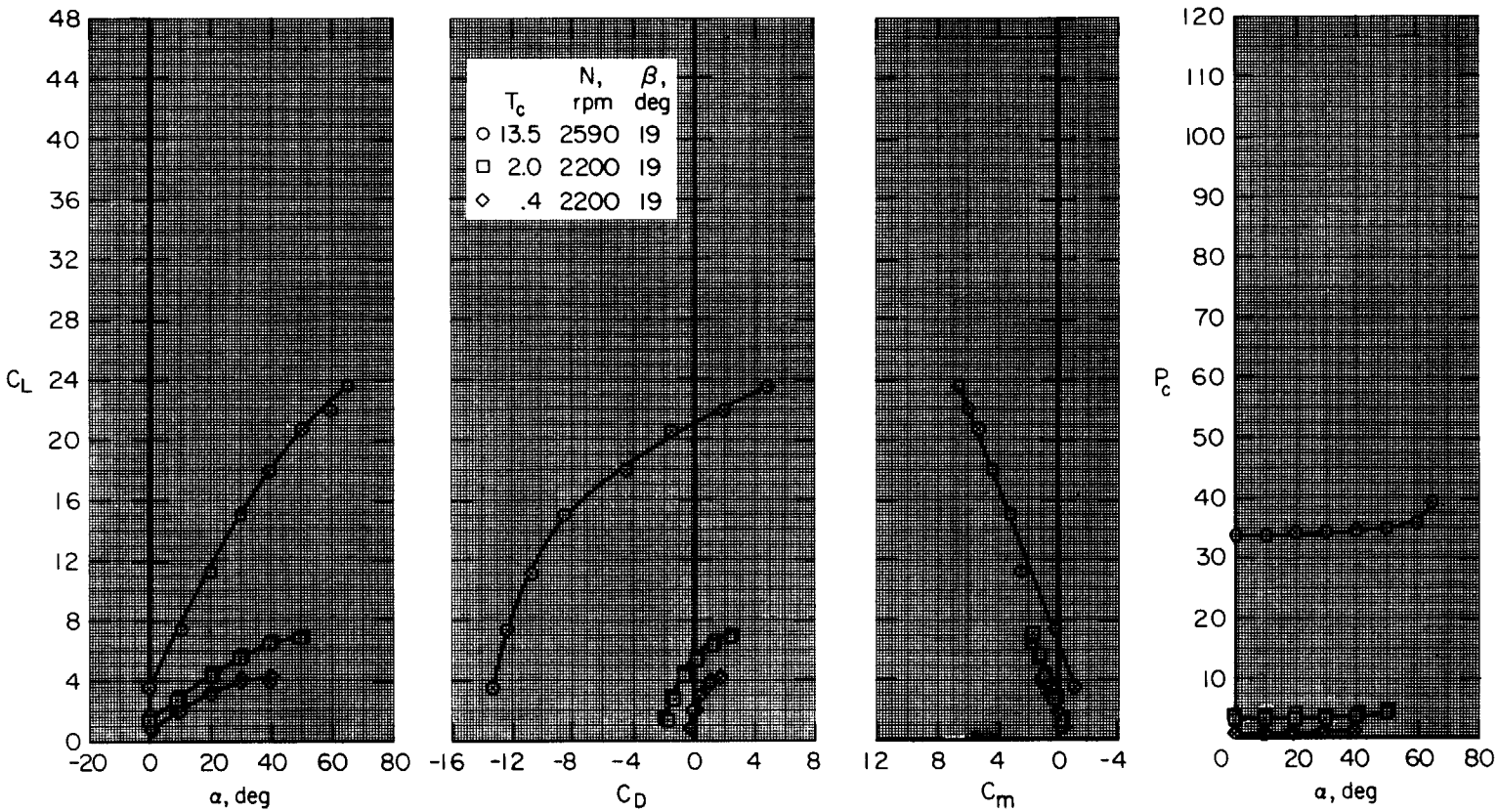

(f) $\delta_V = 20^\circ$

Figure 7.- Concluded.

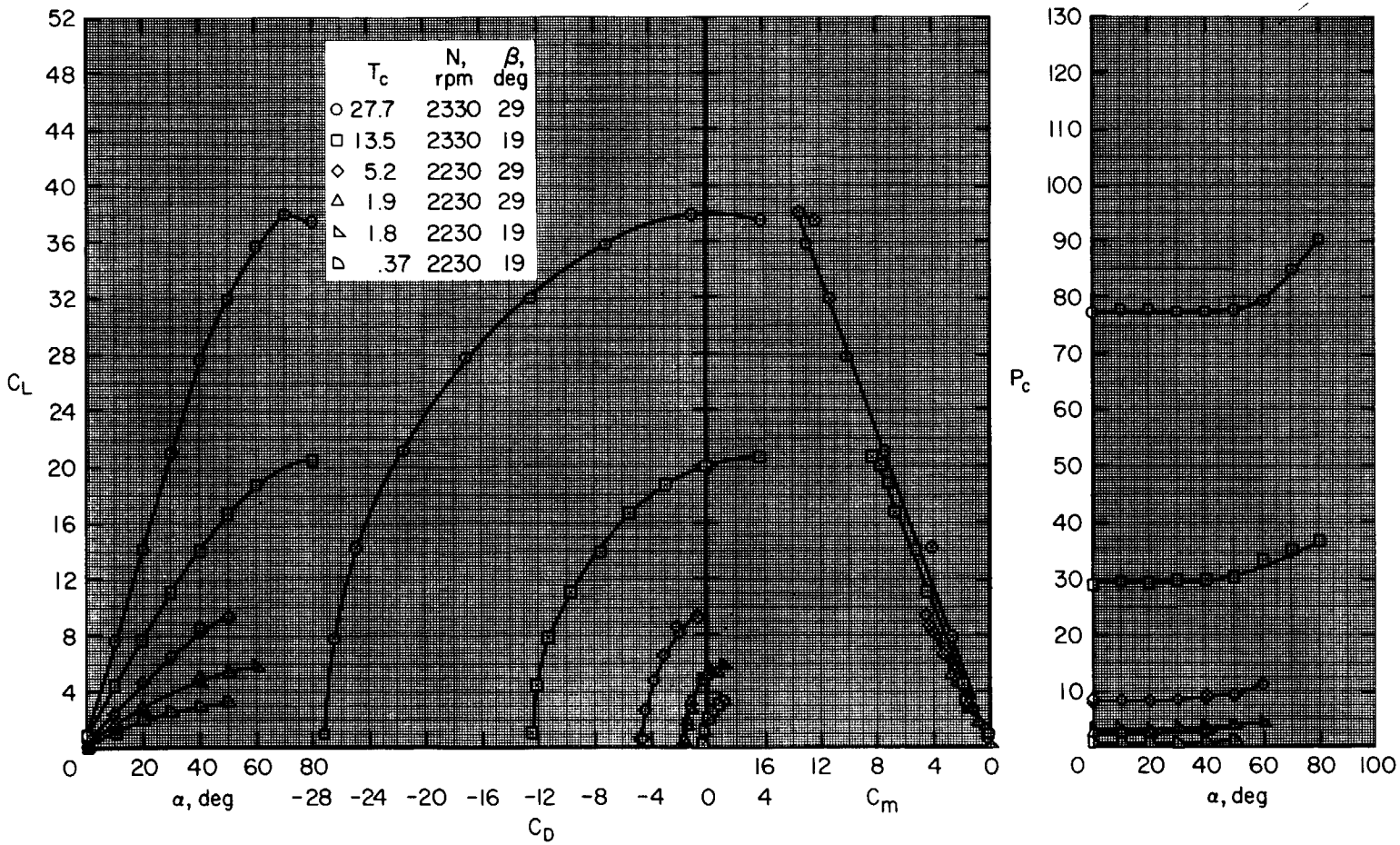

Figure 8.- Aerodynamic characteristics with the exit vane out.

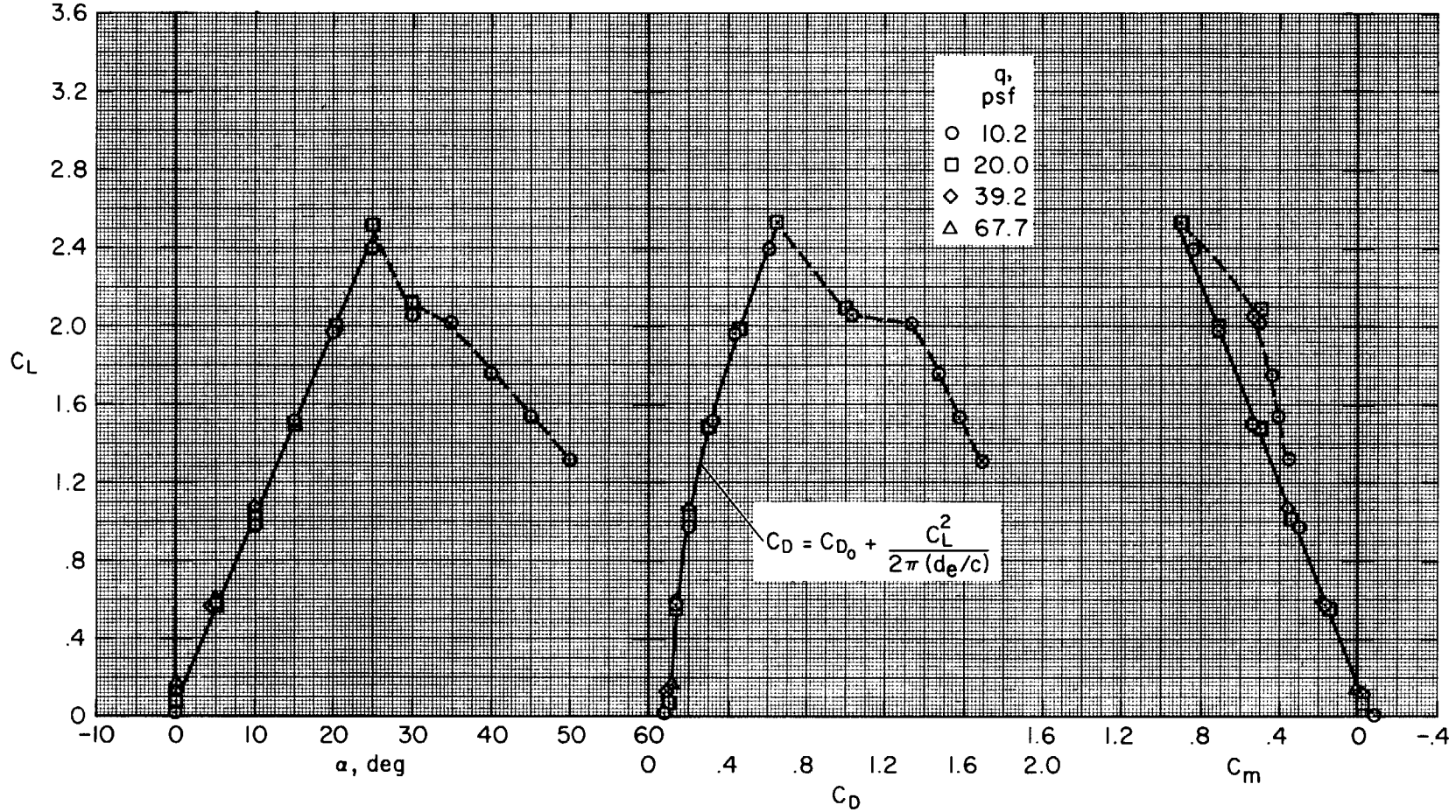

Figure 9.- Aerodynamic characteristics with the propeller removed; $\delta_v = 0^o$.

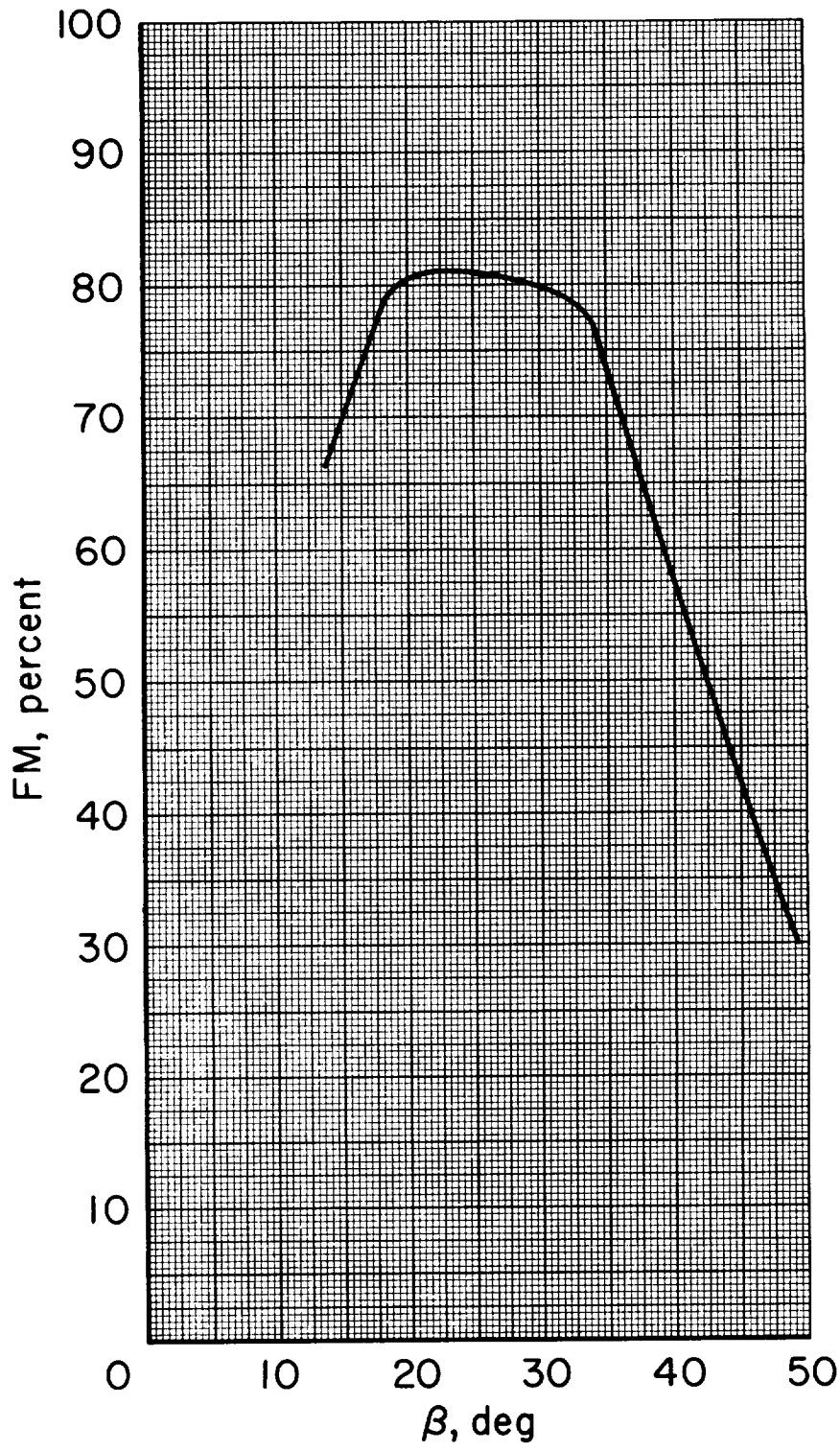

(a) Figure of merit as a function of blade angle.

Figure 10.- Figure of merit and propulsive efficiency computed from the curves of figure 4.

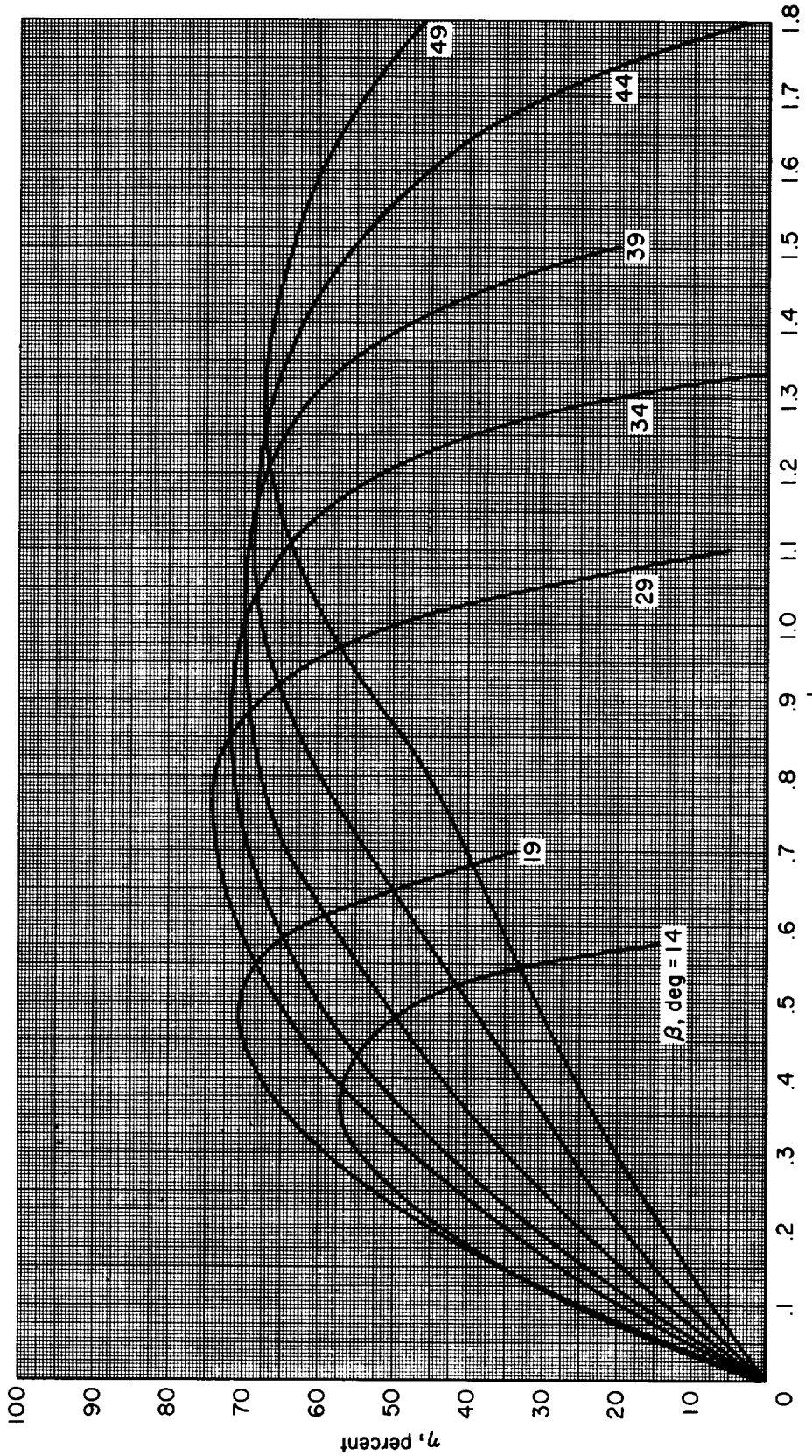

(b) Propulsive efficiency as a function of advance ratio for several blade angles.

Figure 10.- Concluded.

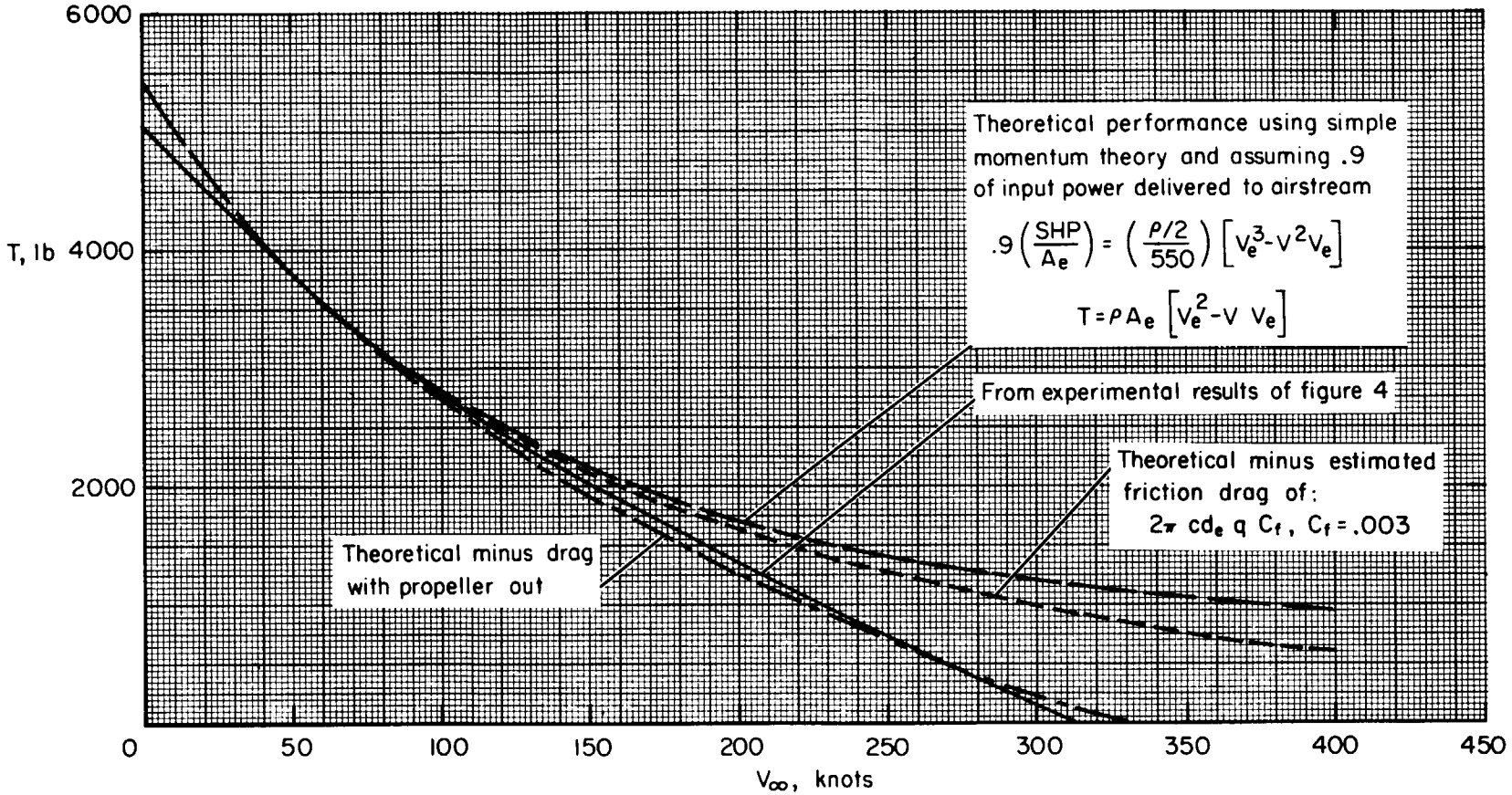

Figure 11.- Thrust as a function of free-stream velocity for a constant power of 1250 hp.

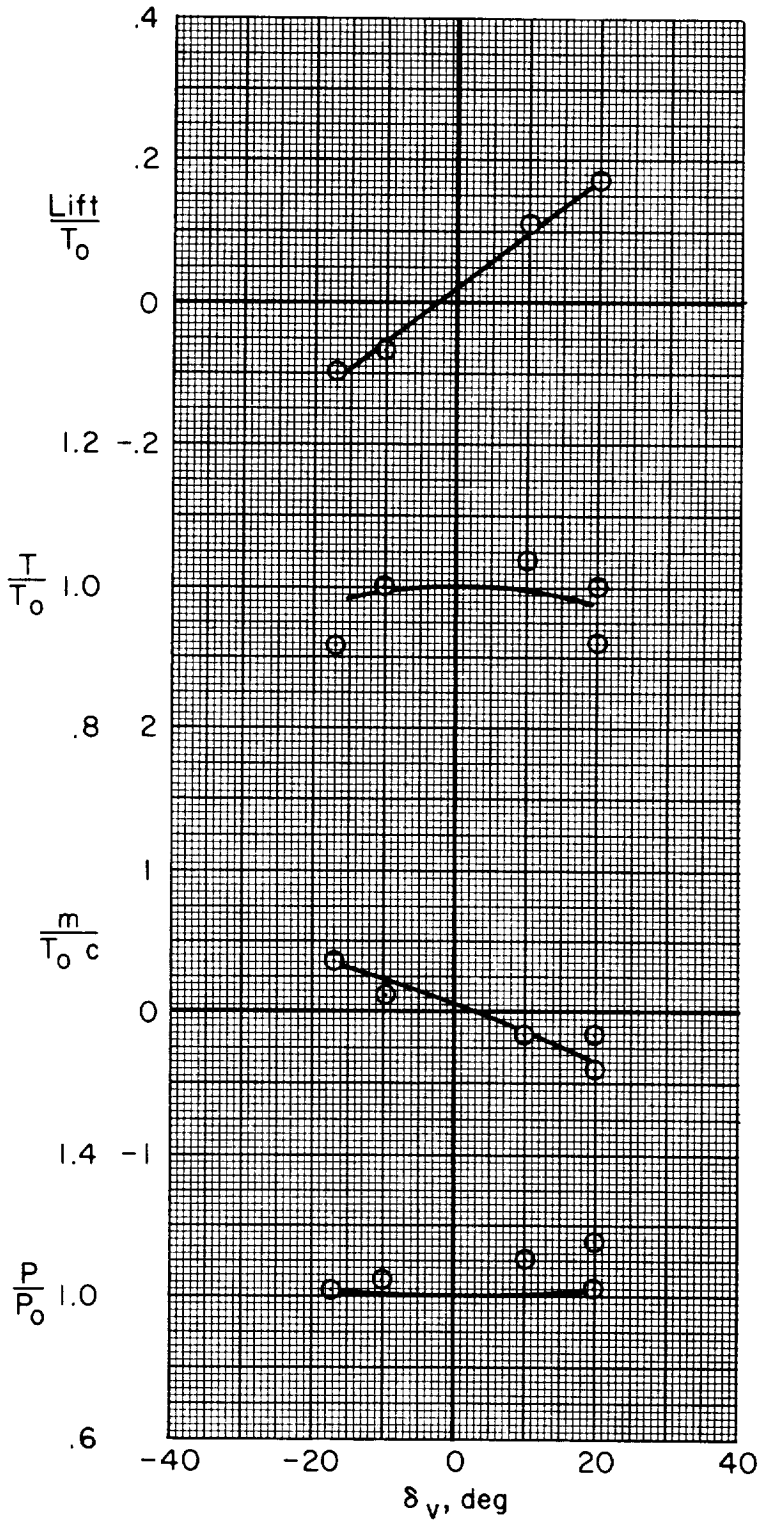

Figure 12.- Effects of exit vane deflection on the aerodynamic characteristics at zero free-stream velocity; $\alpha = 0^{\circ}$, $\beta = 19^{\circ}$.

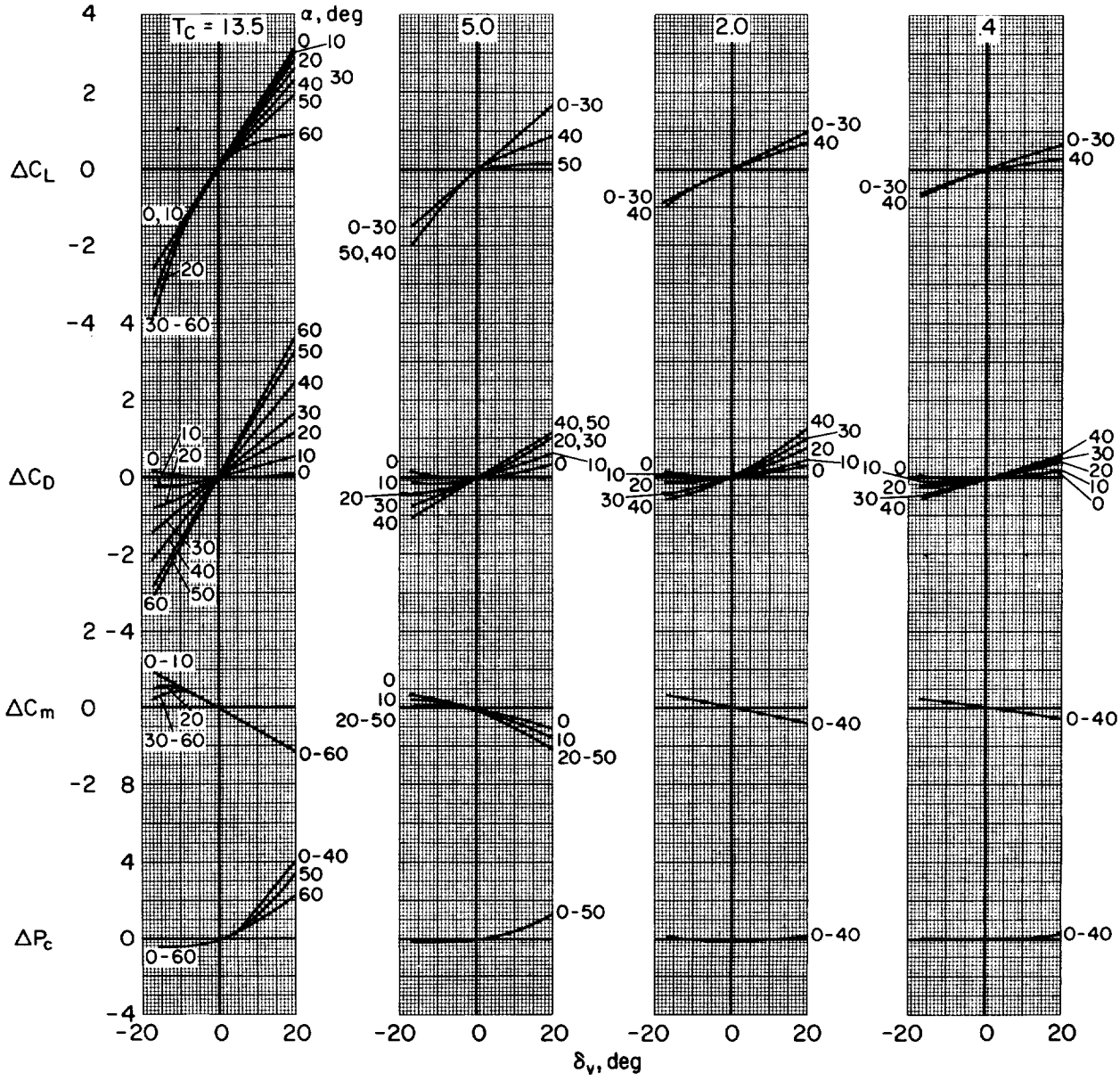

Figure 13.- Summary of exit vane aerodynamic characteristics determined from the results of figure 7 for several thrust coefficients; ΔC_L defined as C_L less C_L at zero vane deflection; ΔC_D, ΔC_m, and ΔP_c similarly defined.

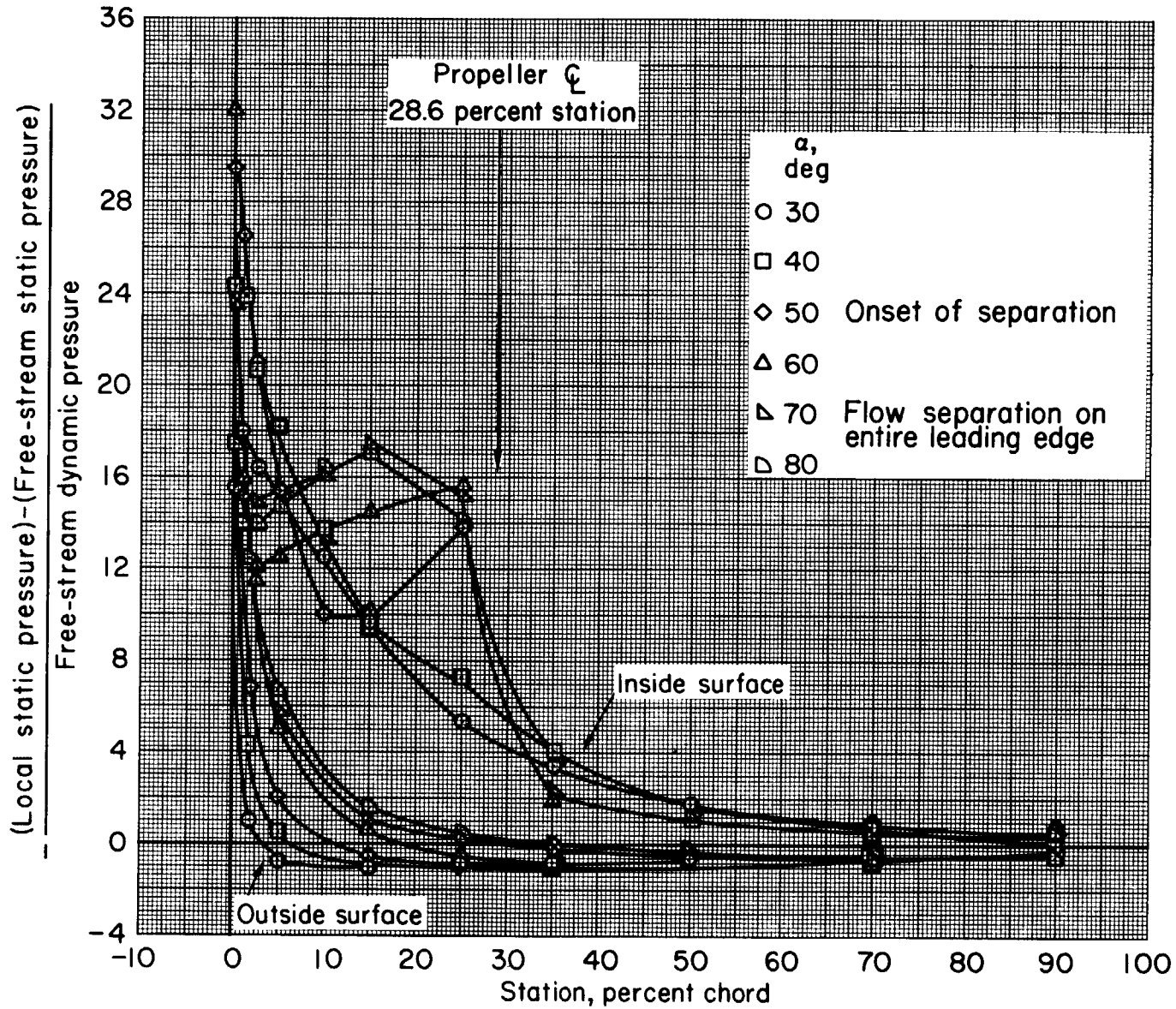

Figure 14.- Typical pressure distributions before and during flow separation on the inside surface of the upstream lip; T_c = 5.0, N = 1806 rpm, and $\beta = 19^{\circ}$.

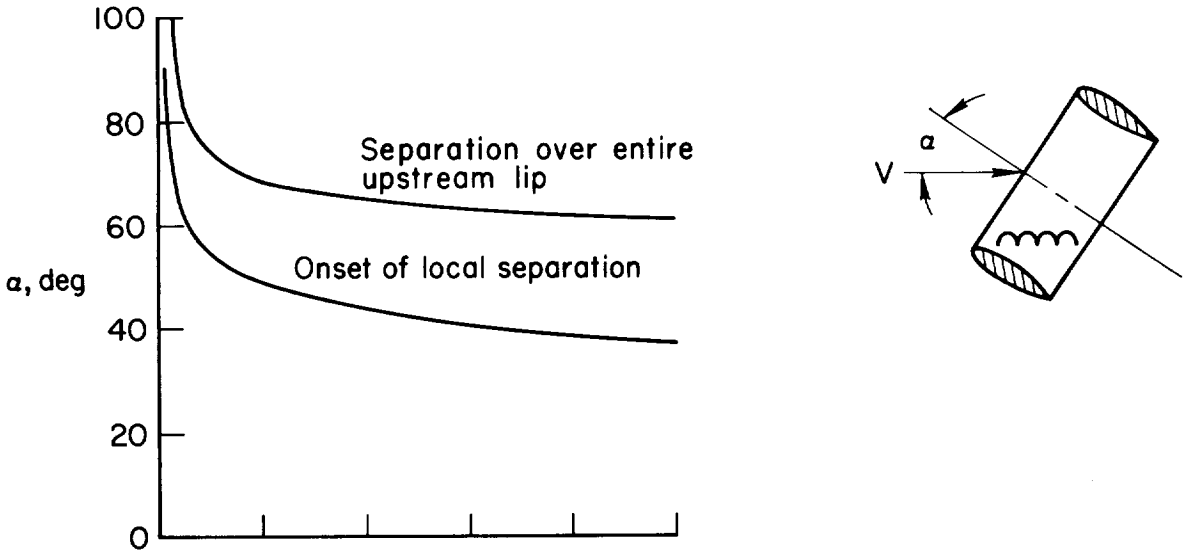

(a) Lip stall for the 7-foot-diameter model.

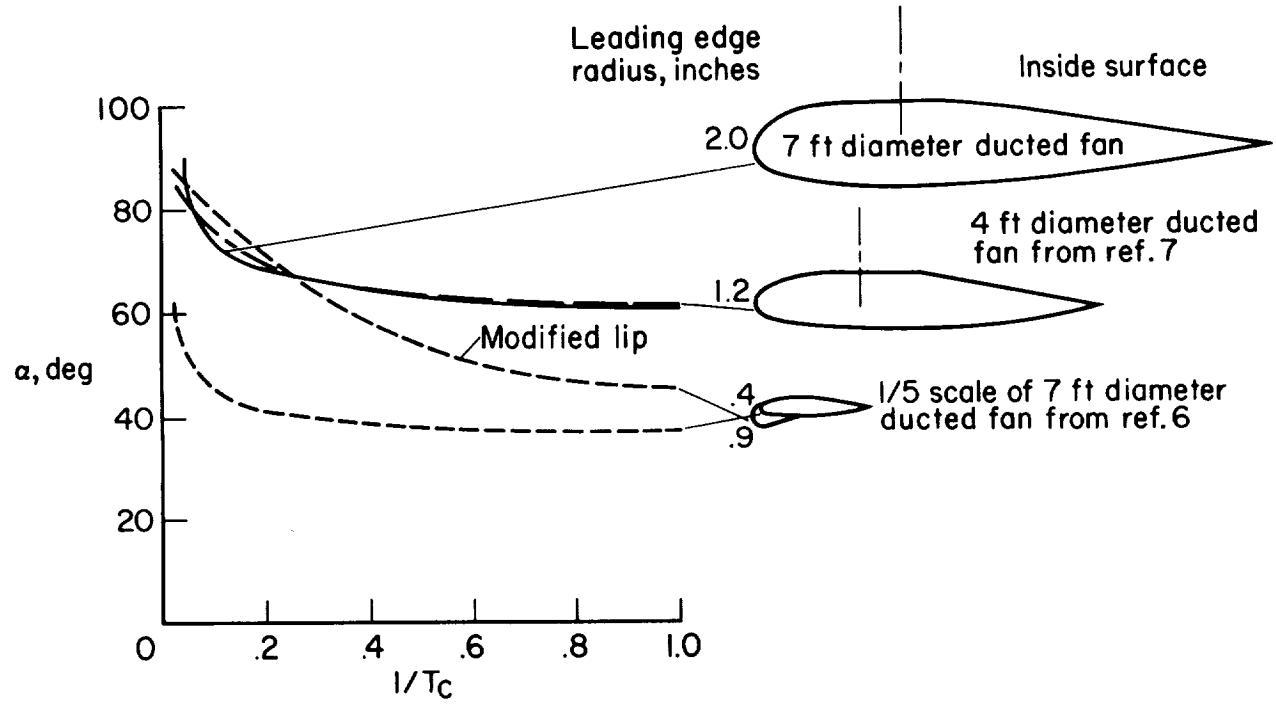

(b) Comparison with other models of conditions at which separation occurred on the entire upstream lip.

Figure 15.- Angle of attack at which stall of the lower or upstream duct lip occurs.

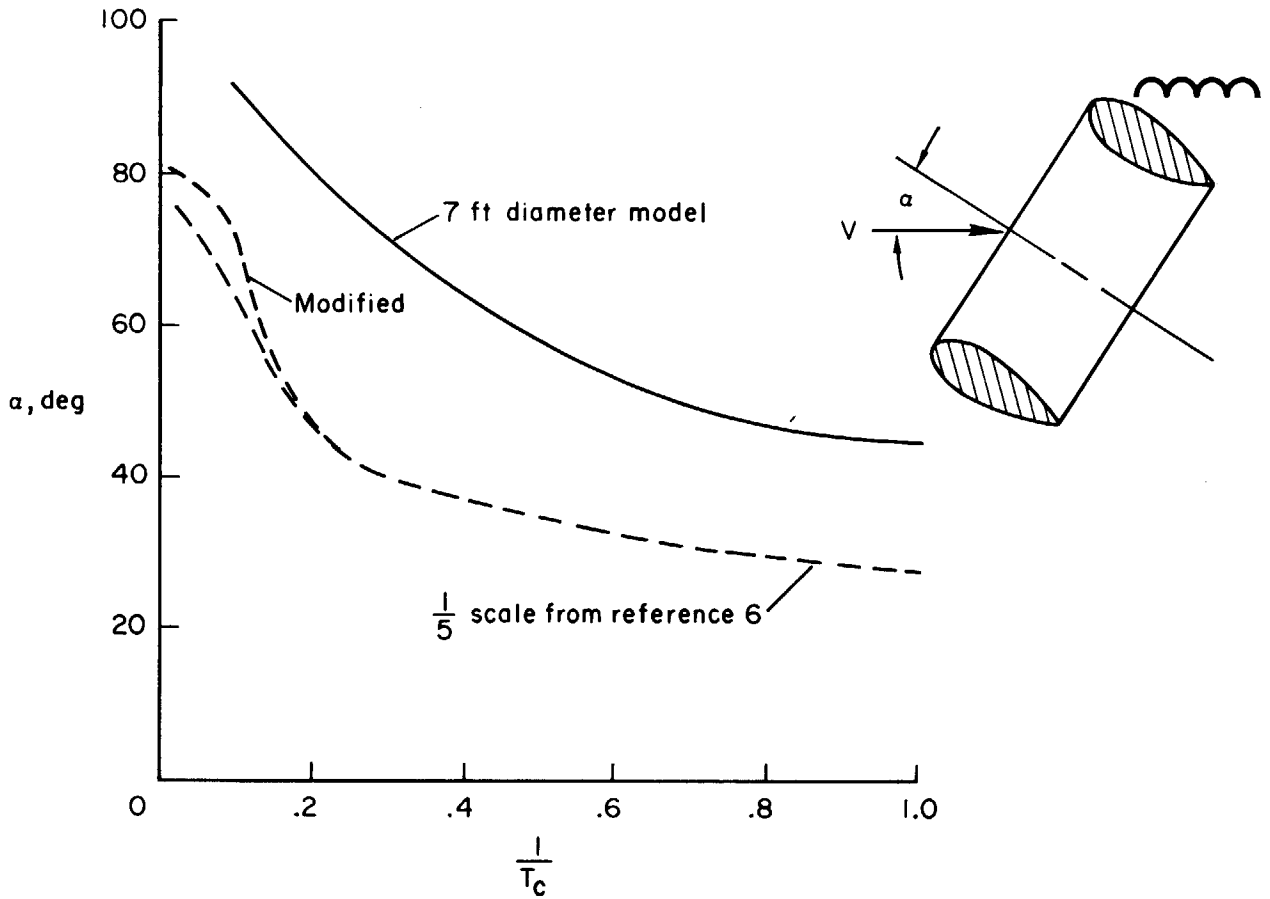

Figure 16.- Angle of attack at which separation occurs on the entire upper or downstream duct lip.

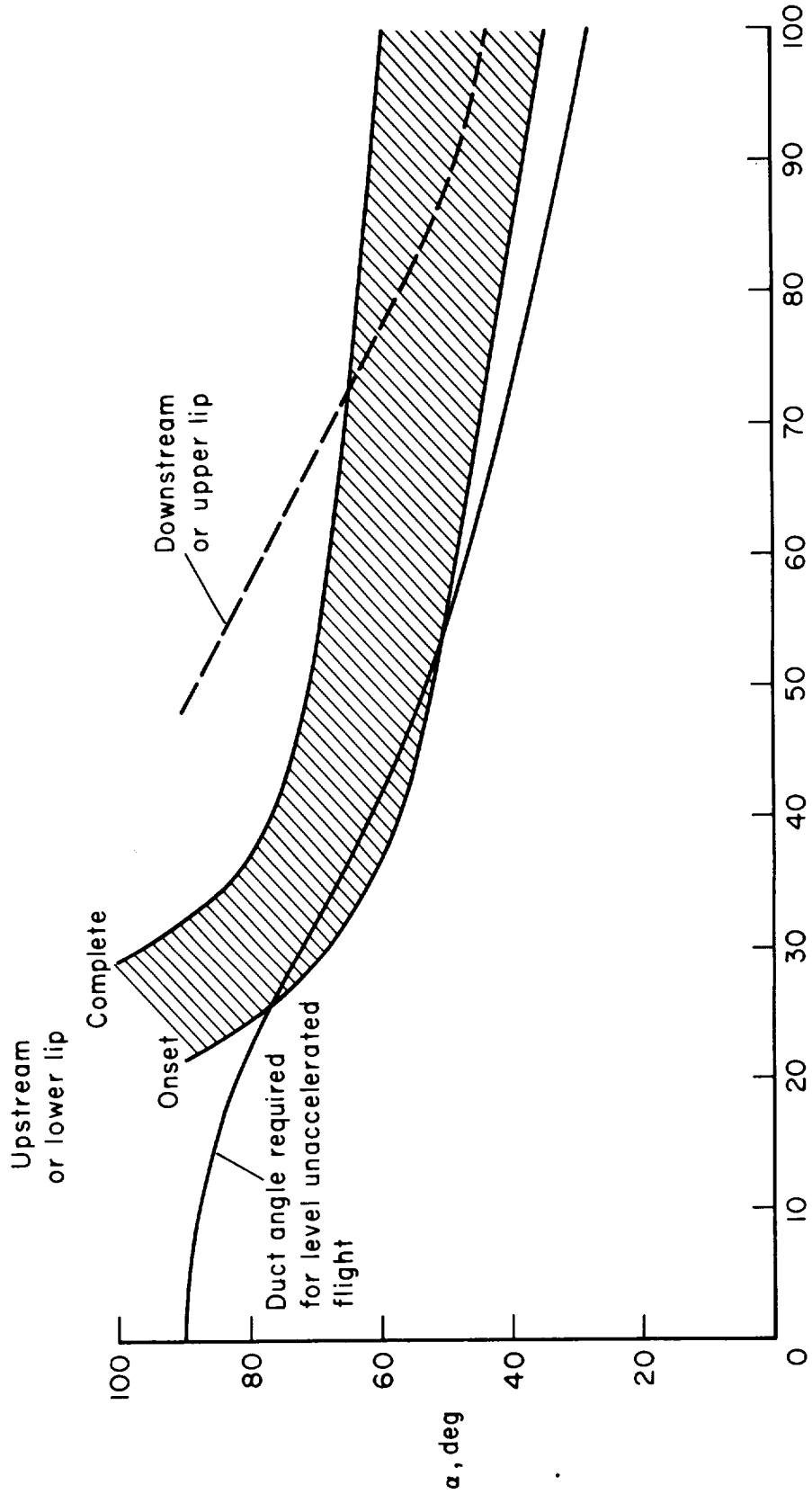

Figure 17.- Predicted duct lip stall angles for the four ducted propeller V/STOL configuration of references 5 and 6.

NASA-Langley, 1967 —— 1 A-2511

9/11/67

"The aeronautical and space activities of the United States shall be conducted so as to contribute . . . to the expansion of human knowledge of phenomena in the atmosphere and space. The Administration shall provide for the widest practicable and appropriate dissemination of information concerning its activities and the results thereof."

—NATIONAL AERONAUTICS AND SPACE ACT OF 1958

NASA SCIENTIFIC AND TECHNICAL PUBLICATIONS

TECHNICAL REPORTS: Scientific and technical information considered important, complete, and a lasting contribution to existing knowledge.

TECHNICAL NOTES: Information less broad in scope but nevertheless of importance as a contribution to existing knowledge.

TECHNICAL MEMORANDUMS: Information receiving limited distribution because of preliminary data, security classification, or other reasons.

CONTRACTOR REPORTS: Scientific and technical information generated under a NASA contract or grant and considered an important contribution to existing knowledge.

TECHNICAL TRANSLATIONS: Information published in a foreign language considered to merit NASA distribution in English.

SPECIAL PUBLICATIONS: Information derived from or of value to NASA activities. Publications include conference proceedings, monographs, data compilations, handbooks, sourcebooks, and special bibliographies.

TECHNOLOGY UTILIZATION PUBLICATIONS: Information on technology used by NASA that may be of particular interest in commercial and other non-aerospace applications. Publications include Tech Briefs, Technology Utilization Reports and Notes, and Technology Surveys.

Details on the availability of these publications may be obtained from:

SCIENTIFIC AND TECHNICAL INFORMATION DIVISION

NATIONAL AERONAUTICS AND SPACE ADMINISTRATION

Washington, D.C. 20546